Experimental Hydrocephalus:

Novel Injection Methods

and

Investigations of Blood-Brain Barrier Disruption

by

Ili Slobodian

A Thesis Submitted to the Faculty of Graduate Studies of

The University of Manitoba

in Partial Fulfilment of the Requirements for the Degree of

MASTER OF SCIENCE

Department of Pathology

University of Manitoba

Winnipeg, Manitoba

Experimental Hydrocephalus: Novel Injection Methods and Investigations of Blood-Brain Barrier Disruption

BY

Ili Slobodian

A Thesis/Practicum submitted to the Faculty of Graduate Studies of The University of Manitoba in partial fulfillment of the requirement of the degree

Of

MASTER OF SCIENCE

Table of Contents

Abstract

Hydrocephalus is a common neurological condition characterized by an imbalance between the production and drainage of cerebrospinal fluid (CSF) within the brain. This results in enlargement of the ventricular system, leading to compression, stretching and damage of axons and the surrounding brain tissue. The current method of hydrocephalus induction in small laboratory animals is to inject kaolin (aluminum silicate) into the cisterna magna. The goals of the experiments described in this thesis are to evaluate and further investigate this method.

Our first goal was to develop a non-inflammatory model of hydrocephalus in rats, using alternative protein and synthetic biopolymers. We hypothesized that at least one of the agents tested would be as efficacious as kaolin for induction of hydrocephalus in young rats, as there is evidence in the current literature that these agents were non-inflammatory when used in surgical techniques or cell-culture. Our second goal was to induce hydrocephalus in young and adult CD1 mice using the cisterna magna kaolin injection method. We hypothesized that we would be able to successfully induce hydrocephalus in young and adult CD1 mice using kaolin, and that the results would be similar to those seen in the rat model. Our final goal was to study blood-brain barrier (BBB) disruption in hydrocephalic rats. Using the kaolin injection method, we hypothesized that there would be some degree of either focal or diffuse BBB disruption in the hydrocephalic state. We hypothesized that this disruption would be evident on Gadolinium-contrast

enhanced T1 weighted MR imaging and that there would be corresponding evidence of disruption upon histological analysis.

We found that none of the compounds tested were as effective as kaolin in inducing hydrocephalus in rats, therefore kaolin should currently remain the gold standard. We were successful in inducing hydrocephalus in adult and young CD1 mice with kaolin and have described effective induction parameters for this method. Vascular tracer studies and magnetic resonance imaging were conducted to test the hypothesis that hydrocephalus leads to disruption of the blood brain barrier. Although we found foci of barrier breakdown after hydrocephalus induction, the sites were found to be random and unpredictable in location.

We believe that these results provide answers to some of the questions proposed in the literature regarding the efficacy of the current kaolin model and whether the blood brain barrier becomes disrupted as a result.

Acknowledgements

I would first like to thank my supervisor Dr. Marc Del Bigio for accepting me into his lab and providing me the opportunity to learn and explore the world of research. He has been extremely patient and understanding throughout my tenure and his door was always open. Thank you for your constant support.

I also need to thank all of the members of the Del Bigio lab for their support and assistance. A special thank you to Terry Enno who has continuously directed and assisted in me in every aspect of my laboratory work, and thank you to Dr. Richard Buist for his assistance with MR imaging. Thanks to Angela Schellenberg for teaching me how to use the MRI programs, and thank you for assisting with MR imaging and performing all the contrast calculations for the dextran experiment. Thanks to Dmitri Krassioukov-Enns for assisting with the biopolymers experiment and for creating all of the figures. A big thank you to Dr. Luiza Lopes for assisting me with all of the crazy mouse behavior tests and for constantly checking on our little men. But mostly, thank you so much for rescuing my mouse data after my hard drive crashed.

My family has provided me with their undying love and support. I would not have attempted this project without them. Thanks to my parents who went above and beyond the call of duty as grandparents, caring for Carmen as I worked on experiments and my thesis. A very special thank you to my husband Darren who provided me with his love, support and stability throughout some very hectic times. I could not ask for a better partner.

To Ashley and Jeff: thanks for coffee, lunch, after lunch coffee, dinner, after dinner coffee and all the coffee breaks that fall in between. Without you guys, I would have given up before it had even started. Thanks for all the study sessions, the class notes and the answers to all of my questions. Thanks for being my sounding board, my complaint department and my audience. To Jody, thanks for all of your advice. You are my inspiration & my comic relief. Thanks for listening. I miss you, please come home.

Finally, I would like to extend a big thank you to the members of my committee, Dr. Yvonne Myal and Dr. Mark Torchia, for their time, patience and continued support.

Abbreviations

ANOVA	Analysis of variance
BBB	Blood-brain barrier
BSA	Bovine serum albumin
BUI	Brain uptake index
° C	Degrees Celsius
CBF	Cerebral blood flow
CNS	Central nervous system
CRASH	X-linked human congenital hydrocephalus
CSF	Cerebrospinal fluid
CT	Computed tomography
CVO	Circumventricular organs
DMSO	Dimethyl sulfoxide
EHS	Engelbreth-Holm-Swarm
EVOH	Ethylene vinyl alcohol
FGF2	Fibroblast growth factor type 2
FITC	Fluorescein-isothiocyanate
FITC-D	Fluorescein-isothiocyanate dextran
Gd	Gadolinium
Gd-GTPA	Gadolinium diethylenetriamine penta-acetate
H&E	Hematoxylin and eosin
HRP	Horseradish peroxidase

ICP	Intracranial pressure
MR	Magnetic resonance
MRI	Magnetic resonance imaging
MRPs	Multidrug resistance proteins
MS	Multiple sclerosis
NBCA	N-butyl-cyanoacrylate
NSF	N-ethylmalemide-sensitive factor
OATs	Organic ion transporters
PBS	Phosphate buffered saline
PBST	Phosphate buffered saline tween-20
PET	Positron emission tomography
QAR	Quantitative autoradiography
RISA	Radio-iodinated serum albumin
ROI	Region of interest
TGF-1	Transforming growth factor-1
TGF-beta	Transforming growth factor beta

List of tables and figures

Chapter 1: Introduction

Chapter 1: Introduction

1.1: Background

Hydrocephalus is a common neurological condition characterized by an imbalance between the drainage and production of cerebrospinal fluid (CSF) within the brain. This imbalance results in enlargement of the ventricular system, leading to compression, stretching and damage of axons and the surrounding brain tissue [1]. As the fluid volume increases, pressure increases within the intracranial vault. The most common causes of this condition are an obstruction to the CSF flow somewhere within the ventricular system, thus impeding drainage; or an imbalance between CSF production and reabsorption.

1.2: Cerebrospinal Fluid

Cerebrospinal fluid is produced by the brain and acts as a buffer and a cushion. It also acts as a reservoir for waste products such as amino acids and lactate which are formed in the brain [2-4]. CSF is formed at the rate of 10-20mL/h by two main sources, the choroid plexus in the ventricles (~80%) and by the products of metabolism within the brain itself [3, 5, 6]. The capacity of the lateral and third ventricles in a healthy adult human is 20mL and the total volume of CSF including the cranial and spinal subarachnoid compartments is roughly 120mL. The CSF flows through the ventricles into the subarachnoid space and over the entire surface of the brain in a predictable pathway.

From the choroid plexus in the lateral ventricles, CSF flows through the intraventricular foramen of Monro and into the third ventricle, then via the cerebral aqueduct into the fourth ventricle. From the fourth ventricle CSF flows through the two lateral foramina of Luschka and then via the single midline foramen of Magendie, into the subarachnoid space, the arachnoid granulations, the dural sinus, and finally into venous drainage [8]. The greatest volume of CSF is absorbed into the bloodstream by the arachnoid villi in the superior sagittal sinus in the subarachnoid space [8].

There is also increasing literature documenting CSF absorption into the lymphatic system adjacent to cranial and spinal nerves [9, 10]. Although the CNS parenchyma does not contain lymphatic vessels, studies suggest that there is a physiological link between cerebral interstitial fluid, CSF and extracranial lymph [10]. Studies using protein tracers injected directly into brain interstitium or CSF, exit the cranium along prolongations of the subarachnoid space associated with cranial nerves, and enter lymphatic vessels [10]. These tracer studies have shown that extracranial lymphatics play an important role in CSF transport in both the fetal and adult brain. Volumetric quantitative studies suggest that almost one-half of all CSF removed from the cranium is cleared by lymphatics [10, 11]. Elevations of intracranial pressure (ICP) also lead to increased CSF transport into cervical lymphatics [10, 11]. Therefore it is logical to assume that an interruption of CSF lymph transport would lead to a change in cranial physiology, and relate to the pathogenesis of hydrocephalus.

1.3: Hydrocephalus

Hydrocephalus can develop from a variety of etiological factors including a physical obstruction of the CSF circulating pathways, a reduction in the ability to absorb CSF, or very rarely from over-production of CSF [8]. Mechanisms for these disruptions of CSF flow include congenital malformations, tumors, viral infections, after premature birth or birth trauma [8]. Current research finds hydrocephalus to be one of the most frequent congenital malformation of the nervous system, second only to spina bifida, occurring in an estimated 1/1500 live births [12]. Hydrocephalus also develops in 80% of patients with spina bifida [13], and in 15% of premature (<30 weeks) infants following intraventricular hemorrhage [14].

For descriptive purposes, hydrocephalus has been classified as either internal or external, communicating or non-communicating, etc, depending on where the block to the CSF flow is located [15]. Communicating hydrocephalus occurs when full communication still exists between the ventricles and subarachnoid space [16]. It is most often caused by defective absorption of CSF, due to functional impairment of the arachnoid granulations, which reabsorb the CSF back into the venous system. Communicating hydrocephalus can also stem from an insufficiency of venous drainage [15]. On rare occasions it caused by an overproduction of CSF due to tumors of the choroid plexus. Noncommunicating hydrocephalus occurs when CSF flow is obstructed within the ventricular system or within its outlets to the arachnoid space, thus resulting in ventricular/subarachnoid space non-communication [16]. This 'obstructive'

hydrocephalus usually results from a physical obstruction of the flow of CSF, either intraventricular or extraventricular. Most hydrocephalus is "obstructive", and this term is used to contrast hydrocephalus caused by overproduction of CSF [15].

Specific anatomical sites are susceptible to different types of obstructions. The inter-ventricular foramen can develop tumors or cysts which can impede CSF outflow from the lateral ventricles [7, 16]. Aqueductal stenosis may occur from a congenital malformation or may be obstructed by a number of genetically or acquired lesions (e.g., atresia, ependymitis, hemorrhage, tumor, post-inflammatory scarring) [17]. The fourth ventricle outlets are subject to malformations or obstructions such as congenital stenosis or stenosis from tumors, as well as scar tissue impediment from hemorrhage or post-infection [17]. The subarachnoid compartment can be affected by trauma, hemorrhage or post-meningeal infection scarring, which all may cause damage or obstructions leading to the development of hydrocephalus [18, 19]. Congenital vascular malformations or a decrease in venous absorption can also result in raised venous pressure which can impede CSF outflow and lead to the development of hydrocephalus [7, 17]. In children, meningitis and intrauterine infections affecting reabsorption are the second most common causes of hydrocephalus, after congenital developmental disorders (aqueductal stenosis, myelomeningiocele, Dandy-Walker, encephalocoele) [15-17].

Regardless of the specific cause of hydrocephalus, the effects remain consistent: enlarged ventricles, followed by atrophy of the periventricular white matter and damage to axons.

1.4: Clinical consequences

The clinically relevant signs and symptoms of hydrocephalus depend on the age of the individual and the rate of ventricular enlargement. Initially there is an increase the intracranial pressure (ICP) [7, 8]. The ICP rises if CSF is overproduced, its flow is obstructed or the resorption is disrupted. A small amount of compensation for this imbalance may occur through transventricular absorption of CSF and also by absorption along nerve root sleeves. As the CSF volume continues to increase, the temporal and frontal horns dilate first, which may result in elevation of the corpus callosum, leading to stretching or perforation of the septum pellucidum, thinning of the cerebral cortex, and enlargement of the third and fourth ventricles. In infancy, indications of raised ICP are enlarging head circumference, since skull sutures will move and expand, compensating for the increase in pressure. Although the infant may initially be asymptomatic, as the ICP progressively rises the infant may become irritable, show failure to thrive, vomit, and develop irregular respirations with apneic periods [7, 8, 20]. These symptoms may accompany a full and bulging fontanel in addition to other neurologic signs such as 6^{th} nerve palsy, ataxia, spasticity, tremor, chronic "fisting", "setting-sun" appearance of the eyes, as well as increased or exaggerated deep tendon reflexes and muscle tone in the lower extremities [8, 17, 20]. Children may also experience endocrine abnormalities such as growth retardation, particularly of the head and trunk regions, and precocious puberty. There are most likely secondary to hypothalamic dysfunction and chronic displacement and stretching of the pituitary stalk [16, 17, 20].

In older children and adults, symptoms of hydrocephalus most often include headaches, nausea and vomiting, lethargy and irritability [21-23]. Older children often experience decreased mental cognition which often presents as deteriorating performance in school, mild memory deficits, a loss of complex cognitive functions, and on occasion, mild dysmetria of the extremities [20]. Individuals with chronic hydrocephalus most often experience mild weakness of the upper extremities and gait disturbances, possibly related to stretching of the corticospinal fibers [20, 21, 23].

Treatment for hydrocephalus usually involves surgical interventions to either place a shunt to drain the CSF into other body cavities (e.g. into the peritoneum), or to perform a third ventriculostomy, which creates a hole in the floor of the third ventricle, creating a detour around the blockage to allow the CSF to circulate and be reabsorbed [24].

1.5: Pathology and Pathogenesis

Brain injury from hydrocephalus is multifactorial and complex. The pathological changes caused by hydrocephalus have been reviewed in detail [25-29]. In summary, CSF flow is impeded, the cerebral ventricles dilate, thus causing physical, biochemical and cellular changes within brain parenchyma.

Ependyma and the subventricular zone

The ependyma is a simple epithelial cell layer that covers the surface of the ventricles in the brain and the central canal of the spinal cord. The cells are cuboidal/columnar in morphology and their apical surface contains a cluster of cilia, which help circulate the CSF around the CNS [30]. Cells in the choroid plexus are modified ependymal cells that lie over a capillary network; this organ secretes CSF. Several animal models of hydrocephalus have been attributed to ependymal or ciliary dysfunction [31-34]. Ciliary function in the ventricular system is also important in humans, as evidenced by the increased incidence of hydrocephalus in human patients with primary ciliary dyskinesia [34, 35].

Light and electron microscopy studies have shown a consistent array of pathological changes associated with the development of hydrocephalus. These changes have been found to correlate with the sequence, severity and extensiveness of the ventricular dilation, rather than the mode of induction [30]. The initial stages of tissue damage include flattening, stretching and disruption of the ependymal lining of the ventricles[30, 36-39]. These changes are most often noted along the dorsal and lateral aspects of the lateral ventricles, which are the regions most affected by the increasing surface area of the distending ventricles [30, 38, 40, 41]. This focal denudation of the ependyma can lead to a progressive decrease in the number of cilia present and may lead to widespread cell loss. The ependymal cells proliferate only minimally after induction of hydrocephalus [30, 36, 42].

The subventricular zone is a cell layer beneath the ventricular zone, surrounding the lateral ventricles. This region contains myelinated axons and adult neural stem cells which have the potential to generate new neurons, astrocytes and glial cells. In hydrocephalus, in addition to disrupting the ependyma, there is pronounced edema evident in this white matter region, including within the corpus callosum. However the edema does not normally extend into the regions of the caudate nucleus and thalamus. The predominant cells within the edematous white matter are reactive astrocytes containing myelin debris [26]. As the extracellular volume of the white matter increases, it disrupts the normal architecture of the neuropil and possibly affects the metabolism of the surrounding cells [27]. In hydrocephalus, the subventricular zone becomes disorganized and disrupted [43], and astroglial cells proliferate significantly resulting in a periventricular layer of reactive astrogliosis [1].

Astrocytes and axons

The function of resting astrocytes and microglia are to aid cellular growth and development. When activated by injury, these glial cells release cytokines and chemokines which aid in the recruitment of additional astrocytes and microglia to the injured site [44]. This recruitment leads to astrocytosis and the formation of a glial "scar". Astrocytosis is an abnormal increase in the number and size of astrocytes due to the destruction of nearby neurons. Research has shown that reactive astrocytosis increases in parallel with onset and progression of hydrocephalus [44]. These cells multiply at sites of

CNS damage and lay down a dense network of fibrous scar tissue. This scar has the potential to block the growth of new neuronal processes and may also impede neo-vascularization, therefore inhibiting recovery after injury [44]. This impairment in recovery, partnered with the cell death originally caused by hydrocephalus, may contribute to the neurological deficits experienced by patients [44]. Recent research has shown that through appropriately timed surgical shunting, this gliosis can be controlled or reduced in order to minimize its detrimental effects [45]. The reductions in the number of astrocytes are most likely due to the effective diversion of excess CSF to other sites of absorption, which keeps the ICP levels under control and thus reduces the amount of stretch and compression of the cortex [44].

The effects of this gliosis is not only restricted to the periventricular white matter. It also extends throughout the entire cerebral cortex and the peri-aqueductal area [46]. The corpus callosum becomes thin and atrophic due to the stretching of the lateral ventricles, which can result in perforation of the septum pellucidum, hemispheric disconnection and further axonal injury [1, 27]. In severe cases of hydrocephalus the cortex becomes thin and the basal ganglia become atrophic. Chronic damage to the cerebral cortex results in a reduction of the number of large pyramidal neurons. It has been well documented that the functionality of these neurons is greatly altered in a hydrocephalic state [1, 25, 47].

Most researchers agree that hydrocephalus primarily affects axons and their myelination [1, 25, 27]. With the progression of the disease, axons are stretched and their continuity is disrupted. This eventually results in the death of the axon and breakdown of its myelin sheath, which invokes the astrocytic and microglial reactions. In regions of severe edema, axons may be completely absent and these regions filled with myelin debris [27]. This debris is a granular disintegration of neurofilaments, microtubules and vesicular elements [27]. The ability of axons to regenerate is limited and remyelination does not occur in the absence of functional axons. It is for all of these reasons that hydrocephalus is primarily considered to be a white matter disease.

Cerebral blood flow

There are numerous studies documenting alterations in cerebral blood flow (CBF) in hydrocephalus. Studies using MR imaging [48, 49], positron emission tomography (PET), quantitative autoradiography [50], CT and Doppler ultrasonography methods [51, 52] have all reported changes in cerebral blood flow in hydrocephalus. Multiple animal studies report that hydrocephalus causes reductions in cerebral blood flow due to compression and/or alteration of vessels, which leads to white matter damage, injury to oligodendrocytes and alterations in oxidative metabolism [1, 50, 53-56]. The reduction of cerebral blood flow is often considered to be primarily due to changes in ICP and compression and stretch of the vessels [53, 57]. Reduced CBF can also occur due to a reduction of the number of capillaries [58-60] or narrowing of the vasculature secondary to the meningeal inflammatory response as seen in kaolin-induced hydrocephalus [61].

These changes in blood flow have been noted globally, however it is most often investigated in the inferior and dorsolateral prefrontal cortex, superior temporal lobe, anterior and posterior cingulate gyrus, caudate nucleus, occipital cortex and cerebellum, with the greatest reductions in the frontal cortical areas, caudate nucleus and periventricular white matter [50, 62]. These changes are more prominent in the early stages of hydrocephalus progression while the ventricles are actively expanding [15, 53].

Introduction of a CSF shunt in the early stages of onset has been noted to restore blood flow to affected regions [50, 63-67]. After shunting, the ventricles decrease in size, there is resolution of the periventricular edema, there is a reduced number of astrocytes present and glucose metabolism is corrected [1, 44, 50, 68]. The alterations in cerebral blood flow have been noted to return to normal state spontaneously after 3 weeks (feline model), quite possibly due to the slow rate of ventricular enlargement and the lower ICP at 3 weeks [50]. Despite the normalization of CBF and other physiological parameters, permanent injury even following shunting has been reported [1, 47, 69, 70]. Irreversible changes include only partial restoration of synapses and neuron size [71]. The continuity of the ependymal lining is re-established, however altered [25, 72, 73], and the results of reactive astrogliosis remain, causing vascular constriction and periventricular "stiffness" due to the formation of the glial 'scar' [74, 75]. The larger blood vessels can regain their normal configuration, however this recovery is much slower in affected capillaries [76, 77]. Axons may be restored if the damage is mild and neurons can be restored to their normal appearance [71], however if the axons are severed it is unlikely that they can be

restored [26, 78]. These irreversible and permanent alterations of the neurovasculature may also have consequences on the efficiency of the blood-brain barrier (BBB).

1.6: The Blood-Brain Barrier (BBB)

The blood-brain barrier (BBB) is formed by capillary endothelial cells surrounded by basal lamina and astrocytic perivascular endfeet [79]. Astrocytes provide the cellular link to the neurons, contribute to long-term barrier induction, as well as release of chemical factors that modulate endothelial permeability. The blood-brain barrier is located on the endothelial cells of arterioles, capillaries and veins. The BBB phenotype develops under the influence of associated brain cells, specifically astrocytic glia, and contains more complex tight junctions than other capillary endothelia [3]. The BBB is critical for homeostatic regulation of the brain microenvironment, protecting the brain from fluctuations in plasma composition and from circulating agents such as neurotransmitters and xenobiotics, which are capable of disturbing neural function [3, 79]. It maintains homeostasis within the brain environment through strict transport, metabolic and transport-mediated functions. Minor disruptions of barrier function are probably without clinical consequences, while major disruptions accompany most significant acute brain injuries [3].

The properties that determine the passage of substances across the BBB are the size, lipid solubility, the charge of the substance and whether or not there are specific transporters available [3, 80]. Very small molecules, such as water, are able to cross the

BBB without limitation. Molecules such as nicotine, ethanol and heroin are lipid soluble and thus are able to readily pass though the BBB. Other substances such as glucose and amino acids make use of specific transporters in order to cross the BBB. This pathway is either through facilitated transport or through active transport if energy is required.

There are a few regions where it is advantageous for brain cells to be in direct contact with the body's blood plasma constituents. These regions are termed circumventricular organs (CVOs) and they include the choroid plexus, the area postrema, median eminence, pineal gland, neurohypophysis, supraoptic and paraventricular nuclei [3]. These CVOs are specialized structures of the CNS that lack a BBB, and represent a window through which the autonomic nervous system gains direct information about the status of variables in the systemic circulation. They are unique structures, in that they are extensively vascularized and they possess highly fenestrated capillaries [81]. The functional significance of these regions is to allow free exchange of molecules between the blood and adjacent neurons. The lack of BBB allows direct contact and detection of humoral and neural signals that regulate energy homeostasis [81]. This is an important mechanism for substances such as neuroendocrine hormones that are released from nerve terminals in order to allow entry into the circulation and influence the activity of its target [82].

Pathologies such as stroke, trauma, infectious or inflammatory processes, and brain tumors that result in neuronal damage and degeneration, also involve BBB disruption [83, 84]. Breakdown of the BBB is associated with edema, which is the

abnormal accumulation of fluid in tissues and around cells of the body. It is reasonable to hypothesize that the BBB may be disrupted in hydrocephalus and in turn, be an important event in its pathophysiology.

1.7: BBB and the Use of Tracers to Assess Permeability

It was suggested by Hakim in 1976 that hydrocephalic compression of the brain would result in leakage of intravascular blood out of vessels and into the brain. To date, this hypothesis of impairment of BBB efficacy as a consequence of hydrocephalus, has been investigated by a variety of tracer studies [85-89]. These studies have provided evidence of this phenomenon and have demonstrated diffusional movement of water, tracers and neurotransmitters through the compressed extracellular spaces [90]. Weller and Mitchell (1980) and Ogata et al (1972) used horseradish peroxidase (HRP) (40kDa) as a tracer for electron microscopy and reported no detectable disturbances of the BBB in acute kaolin-induced hydrocephalus [38, 86, 91]. However, Nakagawa (1984) reported widening of interendothelial clefts between the tight junctions of capillaries in kaolin induced hydrocephalic rats in their electron microscopy tracer study using HRP, and also reported the presence of interendothelial vacuoles of more than 200nm in diameter [92]. Follow-up studies showed that small tracers such as microperoxidase (1900Da) and lanthanum ($LaCl_3$, 139 Da) crossed the BBB in hydrocephalic rats [93] although tracers as large as HRP did not [94].

Many studies of blood brain barrier permeability in animal models of disorders other than hydrocephalus have utilized radiological and fluorescent tracer molecules [95]. The introduction of FITC-dextrans by Belder and Granath (1973) enables the identification of permeability changes in microcirculation in normal and diseased states, as has been shown in numerous studies [96-99]. FITC-Ds remain free and solubilized in plasma, since they do not bind to proteins or enter blood cells, and do not move across the normal blood-brain barrier [98-100]. Fluorescein-isothiocyanate (FITC)-dextrans are very useful tracers for studying vascular permeability in nervous tissue, as they are available in a wide range of molecular weights and can be subjected to microscopic and quantitative analysis. Coupling fluorescein-isothiocyanate to dextrans (FITC-D) creates a tracer particle that can be utilized with electron microscopy, fluorescence stereo microscopy and high-powered light microscopy [97]. Therefore, the tracer can be studied *in vivo* during the experiment, as well as during fixation and tissue processing. The permeability of the normal intact blood brain barrier in rats has been previously studied and noted that the capillaries of the cerebral cortex are impermeable to FITC-D tracers as small as 3kDa (2.4nm), Horseradish peroxidase (40kDa, 5nm), Evan's blue (69kDa), and sodium fluorescein (0.4kDa, 0.5nm) [98, 101, 102].

1.8: Animal Models of Hydrocephalus

Animal models of hydrocephalus have many histopathological similarities to humans and they can be used to further understand the genetics and pathogenesis of brain damage [12]. To study the pathogenesis of brain damage, hydrocephalus can be experimentally induced through a variety of techniques. The most commonly used methods involve the placement or injection of a foreign material that occludes CSF outflow and may have a component of inflammation. Materials used include bacteria, blood, cotton, lampblack, kaolin (aluminum silicate), and silicone oil. In order to accurately study the pathophysiology of obstructive hydrocephalic brain damage, the method of induction should cause the ventricles to dilate but should not directly affect the brain, which can be seen in chemical, radiation and viral induction methods [103]. Hydrocephalus can be induced in a wide variety of species including mouse, rat, guinea pig, rabbit, cat, dog, pig, fetal lamb, and primates such as Macaca mulatta and Rhesus monkey [37, 38, 104-107].

1.9: Hereditary Models of Hydrocephalus

Genetic studies in animal models have opened the door to understanding the underlying pathology of hydrocephalus. To date at least 43 gene mutations leading to hydrocephalus have been described in animal models. Ten congenital hydrocephalus genes have been identified, most of which code for important cytokines, growth factors or cell signaling related molecules [12]. However, to date only one human hydrocephalus gene has been

identified. Molecular genetics studies have revealed that the gene responsible for X-linked human congenital hydrocephalus (CRASH) is on the Xq28 chromosome, encoding for the L1CAM protein, a member of the immunoglobulin gene superfamily of neural-cell adhesion molecules [108, 109]. L1CAM plays an important role in neuronal migration, adhesion, neurite outgrowth, fasciculation, and myelination. To date, over 150 mutations in the L1CAM gene have been reported.

1.10: Hereditary Models of Hydrocephalus in Mice

A variety of transgenic mouse models have been shown to spontaneously develop hydrocephalus. The autosomal recessive hydrocephalus-1 (hy1) mouse is characterized by its dome-shaped head and dilatation of the entire ventricular system, which is evident within the first 2 weeks of birth [12]. The hy2 mouse exhibits a more severe phenotypic form of hydrocephalus and is associated with inhibition of growth and sterility [110]. The hy3 mutant, identified in 1943, displays a spontaneous transgenic insertional mutation that results in a lethal communicating hydrocephalic mouse with perinatal onset. Studies of this model suggest that this mutation causes defective CSF reabsorption [111, 112].

Another model is the hyh mouse, which is a lethal recessive mutation in the C57Bl/10J mouse strain. It is referred to as the hydrocephalic with hop gait model. These mice display dramatic morphological changes evident at birth and die postnatally from the progressive enlargement of the ventricular system, attributed to narrowing of the cerebral aqueduct with enlargement of the lateral and third ventricles, encompassed with

a smaller cerebral cortex [113, 114]. The mutated protein in this model is referred to as alpha-SNAP, which is a soluble N-ethylmalemide-sensitive factor (NSF) attachment protein [115].

The neural adhesion molecule L1 is a member of the immunoglobulin superfamily of cell recognition molecules, which plays a pivotal role in nervous system development [116]. Humans with L1 mutations develop a severe neurological disease called CRASH, which leads to X-linked hydrocephalus development. Mice with this same deficiency in L1 display severe hydrocephalus characterized by significant enlargements of the skull and severe atrophy of the cerebral cortex, however without displaying stenosis of the cerebral aqueduct. Both the human and the mouse with this mutation have primary brain malformations in addition to hydrocephalus.

Mice which over-express transforming growth factor-1 (TGF-1) have been found to develop hydrocephalus and the injection of human TGF1 into the subarachnoid space of 10-day old mice also results in hydrocephalus induction. The mechanism of this development seems to be obliteration of the CSF pathways within the subarachnoid space [117-119].

Several mouse models of hydrocephalus have been attributed to ependymal or ciliary dysfunction [31-34]. Disruption of the outer dynein arm protein Mdnah5 in mice, results in impaired cilia motility on ependymal cells. The subsequent reduction of CSF flow is suggested to contribute to aqueduct closure during early postnatal development,

thus leading to development of hydrocephalus [34, 120]. An analogous mechanism may be involved in the WIC-Hyd rats which also have impaired cilia motility [32, 121]. Mice with mutations in the cilia proteins Spag6, polaris, hydin, or in the transcription factor Hfh4, which lack ependymal cell cilia, all develop hydrocephalus as well [34, 111, 122]. Additionally, ciliary dyskinesia is associated with hydrocephalus in rats [121], dogs [123] and humans [124-126].

1.11: Hereditary Models of Hydrocephalus in Rats

The morphological and developmental changes in the ventricular system have been well studied in 2 hydrocephalic rat models; the Hydrocephalus Texas (H-Tx) rat, and the LEW/Jms rat. The H-Tx rat is a homozygous carrier of an autosomal recessive gene with incomplete penetrance [127]. These rats have fetal-onset hydrocephalus associated with narrowing of the cerebral aqueduct, although the precise mechanism that leads to this narrowing is still undefined. The LEW/Jms rat display a similar onset and phenotype to the H-Tx rats [12, 128].

1.12: Mechanical Models of Hydrocephalus

Mechanical models involve the placement or injection of a foreign material that occludes CSF outflow. Dandy and Blackfan first described the induction of hydrocephalus through the injection of lampblack (charcoal soot) into the cisterna magna of adult dogs in 1913 [129]. Other materials that have been successfully utilized for

hydrocephalus induction include bacteria, blood, cotton, lampblack, and silicone oil. Viscous silicone oil causes mild hydrocephalus associated with negligible inflammation, however it is not a reliable method for small animal induction because it is difficult to force through a small-gauge needle [15, 103]. Blood injection directly into the ventricles of young rats can cause hydrocephalus [130]. Unfortunately this directly disrupts brain tissue at the site of injection. We have attempted to induce hydrocephalus by injection of blood into the cisterna magna without success (Del Bigio; unpublished observations). Intracranial injection of growth factors such as fibroblast growth factor type 2 (FGF2) [131-133] and transforming growth factor beta (TGFbeta) [119] cause meningeal fibrosis and hydrocephalus in rodents, but both substances are extremely expensive and each can have direct effects on brain.

1.13: Use of Kaolin

The most widely used method of inducing hydrocephalus is by the injection of kaolin clay particles (aluminum silicate) into the cisterna magna, first described by Dixon and Heller in 1932 [134]. This method is inexpensive, simple, reliable, minimally invasive leaving no visible wound, and to some extent titratable.

Kaolin injected into the cisterna magna, causes an inflammatory response of the leptomeninges and the subarachnoid space around the brainstem and cerebellum, resulting in obstruction at the fourth ventricle outlets [15, 104]. In some respects the

kaolin-induction method mimics hydrocephalus caused by meningitis. However, this model has been criticized for its inflammatory effects.

Macrophages, CD4- and CD8- lymphocytes are evident in the subarachnoid space and, according to one report, in surrounding brain parenchyma [135] although this latter aspect has not been replicated in published literature or in our laboratory. Reactive microglia appear in the white matter surrounding the ventricles [136, 137], but this is independent of the mode of induction. It is conceivable that the kaolin-induced inflammation modifies the brain damage, for example through release of cytokines, and for this reason additional options are desired.

Despite the ease and availability of the kaolin injection model in animals from rodents to primates, the use of mice in the study of experimental hydrocephalus has mainly accomplished by the through use of transgenic/knockout animals. Very recently there have been two studies published describing the use of kaolin with mice to induce hydrocephalus [138, 139], however both of these models used the open incision method which we have found technically difficult. More problematic, the lifespan of these animals has not exceeded five days. An injectable and chronic model would be useful because mice with genetic mutations could then be used to test the role of various proteins in the pathogenesis of hydrocephalic brain damage.

At a 2005 National Institute of Health sponsored workshop titled "Hydrocephalus: Myths, New Facts, and Clear Directions", it was determined that research conducted using animal models should be expanded, and that there is a need for new, refined and more physiologically appropriate animals models [140]. The consensus was that there is the need to develop a non-inflammatory obstructive model of hydrocephalus for research purposes, so that it more adequately describes the effects on the brain. It would also be advantageous to establish this model in mice, so as to make use of the wide variety of transgenics available. These issues will be addressed in the following chapters, as we have attempted to establish new and more appropriate hydrocephalus models in both rats and mice.

1.14: Specific goals and hypotheses:

1. Goal: To establish a non-inflammatory model of hydrocephalus in rats, using alternative protein and synthetic biopolymers.
    a. We hypothesized that at least one of the agents tested would be as efficacious as kaolin for induction of hydrocephalus in young rats, but would not be associated with inflammation.

2. Goal: To induce hydrocephalus in young and adult CD1 mice using the percutaneous cisterna magna kaolin injection method.
    a. We hypothesized that we would be able to successfully induce hydrocephalus in young and adult CD1 mice using kaolin.

3. Goal: To study blood-brain barrier (BBB) disruption in hydrocephalic rats.
    a. We hypothesized that there would be some degree of BBB disruptions a consequence of hydrocephalus.
    b. We hypothesized that this disruption would be evident on Gadolinium-contrast enhanced T1 weighted MR imaging.
    c. We hypothesized that the regions of enhancement seen on MR imaging would correlate with areas of regions of BBB disruption as seen on histological samples.

Chapter 2: Protein and synthetic polymer injection for induction of obstructive hydrocephalus in rats

A version of this has been published in The Journal of Cerebrospinal Fluid Research

Cerebrospinal Fluid Res. 2007; 4: 9.

Abstract

Introduction: The objective of this study was to develop a simple and inexpensive animal model of induced obstructive hydrocephalus with minimal tissue inflammation, as an alternative to kaolin injection. Materials: Two-hundred and two male Sprague-Dawley rats aged 3 weeks received intracisternal injections of kaolin (25% suspension in sterile saline), Matrigel®, type 1 collagen from rat tail, fibrin glue (Tisseel®), n-butyl-cyanoacrylate (NBCA), or ethylene vinyl alcohol copolymer (Onyx-18® and Onyx-34®). Magnetic resonance imaging was used to assess ventricle size. Animals were euthanized at 2, 5, 10 and 14 days post-injection for histological analysis. Results: Kaolin was associated with 10% mortality and successful induction of hydrocephalus in 97% of survivors (ventricle area proportion of total brain area 0.168 ± 0.018). Rapidly hardening agents (fibrin glue, NBCA, vinyl polymer) had high mortality rates and low success rates in survivors. Only Matrigel® had relatively low mortality (17%) and moderate success rate (20%). An inflammatory response with macrophages and some lymphocytes was associated with kaolin. There was negligible inflammation associated with Matrigel. A severe inflammatory response with giant cell formation was associated with ethylene vinyl alcohol copolymer. Conclusions: Kaolin predictably produces moderate to severe hydrocephalus with a mild chronic inflammatory reaction and fibrosis of the leptomeninges. Other synthetic polymers and biopolymers tested are unreliable and cause different types of inflammation.

Introduction

Hydrocephalus is a common neurological condition characterized by enlargement of the cerebrospinal fluid (CSF)-filled ventricles, which leads to damage of surrounding brain tissue [25, 141]. To study the pathogenesis of brain damage, hydrocephalus can be experimentally induced through a variety of techniques [103]. The most widely used method is through the injection of kaolin (aluminum silicate) into the cisterna magna [134]. This method is inexpensive, simple, reliable, minimally invasive leaving no visible wound, and to some extent titratable. Kaolin causes an inflammatory response of the leptomeninges and the subarachnoid space around the brainstem and cerebellum, thus causing obstruction at the fourth ventricle outlets [15, 104]. In some respects the kaolin-induction method mimics hydrocephalus caused by meningitis. This model has been criticized for its inflammatory effects. Macrophages, CD4- and CD8- lymphocytes are evident in the subarachnoid space and, according to one report, in surrounding brain parenchyma [135], although this latter aspect has not been replicated in published literature or in our laboratory. Reactive microglia appear in the white matter surrounding the ventricles [136, 137], but this is independent of the mode of induction. It is conceivable that the kaolin-induced inflammation modifies the brain damage, for example through release of cytokines, and for this reason additional options are desired.

Other materials that have been successfully utilized for hydrocephalus induction include bacteria, blood, cotton, lampblack, and silicone oil. Viscous silicone oil causes mild hydrocephalus associated with negligible inflammation, however it is not a reliable method for small animal induction because it is difficult to force through a small-gauge

needle [15, 103]. Blood injection directly into the ventricles of young rats can cause hydrocephalus [142]. Unfortunately this directly disrupts brain tissue at the site of injection. We have attempted to induce hydrocephalus by injection of blood into the cisterna magna without success (Del Bigio; unpublished observations). Intracranial injection of growth factors such as fibroblast growth factor type 2 (FGF2) [131-133] and transforming growth factor beta (TGFbeta) [119] cause meningeal fibrosis and hydrocephalus in rodents, but both are extremely expensive and themselves can have direct effects on brain.

Our goal was to develop an inexpensive injection model of hydrocephalus in rats with minimal tissue inflammation. We evaluated a variety of protein and synthetic polymers 2-14d after injection. Among them were Matrigel®, collagen I from rat tail, fibrin glue (Tisseel®), n-butyl-cyanoacrylate (NBCA), and ethylene vinyl polymer (Onyx-18 and Onyx-34®). Kaolin was used as the control. Matrigel is a solubilized basement membrane preparation extracted from Engelbreth-Holm-Swarm (EHS) sarcoma cells [143], which at 37°C self-assembles into a gel [144]. We used the growth factor-reduced product, which is composed of laminin (61%), collagen IV (30%), and entactin (7%), with residual TGFbeta, FGF, and tissue plasminogen activator, as well as other growth factors. Collagen 1 is a major extracellular structural protein. As a gel, it can facilitate cell growth in the central nervous system [145]. Fibrin glue is a two-component surgical tissue adhesive used to control bleeding and block CSF leaks [146]. It is composed of fibrinogen and thrombin [147, 148]. NBCA glue is a rapidly polymerizing agent that adheres to vessel walls and surrounding tissue; it is commonly used in endovascular surgical techniques [149]. It has been used to induce hydrocephalus in adult

dogs [150]. Onyx® is an ethylene vinyl alcohol copolymer dissolved in dimethyl sulfoxide (DMSO) and is combined with tantalum granules as a contrast agent. It is a non-adhesive embolic agent that develops into a non-permeable, flexible coagulate in the presence of an ionic environment, such as blood or CSF [151]. We hypothesized that at least one of these agents would be as efficacious as kaolin for induction of hydrocephalus in young rats.

Materials and Methods

Animal preparation

All animals were treated in accordance within the guidelines set by the Canadian Council on Animal Care. The local animal use committee approved the experimental procedures and all efforts were made to minimize the suffering and the number of animals used. Humane endpoints for euthanasia such as reduced mobility, respiratory distress and severe neurological impairment, were established prior to experimentation to avoid unnecessary suffering. Agents or doses with obviously adverse effects were tested only once and then abandoned. Two hundred and two locally bred male Sprague-Dawley rats weighing 45-55g at 3 weeks of age were used. Rats were anesthetized with isoflurane gas (1.5% in oxygen). The head and neck were shaved and the neck was flexed to maximize exposure to the foramen magnum. Under aseptic conditions, a 0.30 ml syringe with 30-gauge needle was used to inject each polymer into the cisterna magna percutaneously; 35μl was the starting volume based on our previous experience with

kaolin. Animals were monitored during recovery from anesthetic, weighed regularly, and observed for signs of neurological impairment. Rats were housed 4-5 to a cage and allowed food and water freely. An overdose of carbon dioxide gas was used to euthanize the animals.

Polymer Preparation

Each polymer was tested in the same manner and all were sterile at the time of administration. The procedures were conducted in 4 batches of ~50 animals per batch. For the control group (10 in each batch), rats received injections of 30-35µl sterile kaolin suspension (250 mg/mL in 0.9% saline; Sigma, St. Louis MO, USA). Fibrin glue was prepared according to the supplier (Tisseel®) (Baxter, Mississauga, Ontario, Canada) by mixing individual freeze-dried components in two separate syringes. The first component consisted of concentrated fibrinogen and aprotinin, and the second component consisted of thrombin and $CaCl_2$. Using the Duplojet applicator supplied, 35-55µl of mixed fibrin glue was injected into the cisterna magna. This procedure was abandoned after 2 batches. Liquid high concentration rat tail collagen I (BD Biosciences, Bedford, MA, USA) with a concentration range of 8-11mg/mL was stored at 5°C until needed. Rats received 30-40µl injections of undiluted collagen at room temperature. This procedure was abandoned after 2 batches. Undiluted NBCA (Vetbond, Sigma; St. Louis MO, USA) was injected at room temperature at volumes of 25-35µl per animal. This procedure was also abandoned after 2 batches. Growth factor reduced Matrigel (BD Biosciences, Bedford, MA, USA) was stored at -20°C prior to use. This product gels at 10°C, therefore it was thawed to liquid

consistency and was injected quickly before polymerization. This procedure was completed in 4 batches of animals with increasing volumes. Volume adjustments for Matrigel were made after the first batch showed partial success with an initial injection volume of 35μl. The second batch received 75μl, while the third and fourth groups received 125μl. Onyx-18 (6% ethylene vinyl alcohol, 94% DMSO, viscosity 18 cps at 40°C) and Onyx 34 (8% EVOH, 92% DMSO, viscosity 34 cps) (EV3 International, Plymouth, MN, USA) injections were conducted in 4 batches. The suspensions were shaken vigorously for 15 minutes prior to use and the syringe was primed with DMSO prior to filling. Animals received 35, 25, or 15μl injections. Note that this was the only non-aqueous agent injected; we did not include a DMSO only control group.

Animals from the first two batches were euthanized 14d after injection. Some animals from the 3rd and 4th batches were randomly selected for earlier euthanasia at 2, 5, and 10d to allow histological analysis of the early changes. The number of rats in each group and at each time point is shown in Table 1.

Magnetic resonance imaging

Magnetic resonance (MR) studies were performed prior to euthanasia using a Bruker Biospec/3 MR scanner equipped with a 21-cm bore magnet operating at a field of 7 Tesla (Karlsruhe, Germany) to obtain T2-weighted images of the brain in the coronal plane. The rats were anesthetized briefly with 1.5–2% isoflurane. These methods have been previously described in detail [152]. Ventricle sizes were blindly assessed on the image slice immediately anterior to the third ventricle by measuring the area of the

ventricles and the area of the brain and calculating the ventricle to brain ratio. Successful induction of hydrocephalus in rats surviving >1d was defined qualitatively as ventricle size obviously greater than the largest control (ventricle area index >0.02).

Histological analysis

After MR imaging, the rats were euthanized with a carbon dioxide overdose, followed by perfusion with 10% formalin through cardiac puncture. The skin was removed and heads were further fixed with the brains in situ in 10% formalin. The heads were decalcified in 10% formic acid for 72h followed by paraffin embedding. We chose to embed the entire head so that we could define the injected agents and resulting changes with respect to the brain and the surrounding meninges and skull. Samples including the cerebellum, cisterna magna and fourth ventricle were then cut into 6μm sections, de-waxed and stained with hematoxylin and eosin, Masson's trichrome (to demonstrate collagen), and Leder stain (to demonstrate chloroacetate esterase activity in neutrophils). Blinded assessments were not possible because the administered agents were macroscopically and microscopically obvious.

Statistics

Mortality rates and hydrocephalus induction success rates were compared to kaolin baseline using Fisher exact test. Ventricle size ratios among successes were compared using ANOVA with Games-Howell post hoc comparisons (which allows for groups of unequal size).

Results

Our initial goal was to use silicone oil (dimethylpolysiloxane), because it has been well documented that there is no inflammatory reaction to the oil in the meninges or ependyma [153]. The use of silicone oil to induce hydrocephalus through cisternal injections has been noted to be effective when used with dogs and rabbits [153]. Go et al (1976) also reports success in using 1000 centistoke viscosity silicone oil to induce hydrocephalus in adult rats of ~200g using this method [154]. We attempted to use 1000 centistoke silicone oil in our study, however initial attempts to aspirate the oil through a 30-gauge needle were unsuccessful. We were able to aspirate the oil through a 27-gauge needle, however this needle was too large for use with young rats of only 45g.

Mortality

Rats tolerated the kaolin, Matrigel, and collagen injections fairly well with acceptable levels of acute mortality (10%, 17%, and 0% respectively died or were humanely euthanized within 24h of injection) (see Table 1 for summary of results). Among the Matrigel subjects, rats with large volumes (125-150µl) died immediately. The rapidly hardening agents were associated with significantly greater mortality. Fibrin glue produced 58% acute mortality (usually within minutes); this was due to rapid formation of a rubbery mass adjacent to the brainstem. NBCA injections seemed to be tolerated well initially with most rats awaking from the anesthetic. However, by 24h 74% had died or were euthanized. We hypothesize that the cause of death of these particular animals

was brain stem compression, as upon brain dissection we found hard glue deposits with sharp edges in the posterior fossa, which likely traumatized the brainstem, once the animals started moving. We saw no evidence of hemorrhage after removal of the brain in this region. There was a combined 36% mortality rate with the Onyx® groups either immediately or within 24h after injection. The majority of deaths were among animals injected with 35μl; mortality was lower with smaller volumes. Regardless of the volume, there was an unusual behavioral response to the ethylene vinyl polymer injections. Upon waking from anesthetic, rats scratched at their face and nose profusely and appeared hyperactive for a few minutes. This could be related to the DMSO solvent. With regard to the high mortality experienced by rats in some groups, we were able to abort planned injections of agents that caused immediate death, but the unanticipated early deterioration of NBCA injections was not detected until a second batch had received injections.

Ventricular Dilatation

Among those rats surviving ≥24h, the ventricle size was determined using MR imaging (Figure 1). There were significant differences between the groups. Kaolin predictably produced a moderate to severe degree of hydrocephalus with a proportionate ventricle size of 0.168±0.018 at 10-14d (see Table 1 for details). Matrigel was associated with a mild degree of hydrocephalus (ventricle size 0.057±0.021). Among the few survivors, ethylene vinyl polymer was associated with ventriculomegaly similar to that from kaolin (0.135±0.016).

Table 1: Summary of polymer injection mortality and ventricular size index

Substance	Total Number Injected	Acute Mortality (a)	Time Points	Number with enlarged ventricles (b)	Ventricle Size Index (c)
Kaolin (30-35µl)	40	4 (10%)	2d	4/4	
			5d	5/5	0.125±0.024
			10d	4/4	
			14d	21/23	0.168±0.018
Matrigel (d)	42	7 (17%)	2d	2/3	
		p=0.520	5d	1/4	0.103±0.020
			10d	1/1	
			14d	3/27	0.057±0.021
				p<0.001	p<0.05
Onyx-18 (e)	29	13 (45%)	2d	1/3	
		p<0.001	5d	0/3	
			10d	0/2	
			14d	0/8	-
				p<0.001	
Onyx-34 (f)	37	10 (27%)	2d	2/6	
		p=0.076	5d	3/5	0.113±0.013
			10d	0/9	
			14d	2/7	0.135±0.016
				p<0.001	
NBCA (25-35µl)	23	17 (74%)	5d	1/1	
		p<0.001	14d	3/5	0.026±0.016
				p=0.091	p<0.05
Tisseel (g)	19	11 (58%)	14d	0/8	-
		p<0.001		p<0.001	
Collagen type1 (30-40µl)	12	0 (0%)	14d	0/12	-
		p=0.562		p<0.001	

a) Statistical comparison to kaolin using Fisher exact test (two-tailed)
b) Enlarged ventricles defined as ventricle area index >0.02. Statistical comparison to kaolin using Fisher exact test (two-tailed) based upon total survivors studied at all time points
c) Ventricle size index calculated on the MR slice immediately anterior the third ventricle, total ventricle area / total brain area. The value shown is for successes only, mean ± SEM. Statistical comparison to kaolin based upon combined 10 day and 14 day data, ANOVA with Games-Howell post hoc intergroup analysis (which allows for different group sizes).
d) 35µl 0/11 successes; 75µl 2/10 successful; 125µl 4/11 successful; 150µl 10/10 fatal
e) 35µl 7/7 fatal; 25µl 1/7 successful; 15µl 0/15 successful
f) 35µl 8/8 fatal; 25µl 5/9 successful; 15µl 2/20 successful
g) 55µl 9/9 fatal; 35µl 2/10 fatal

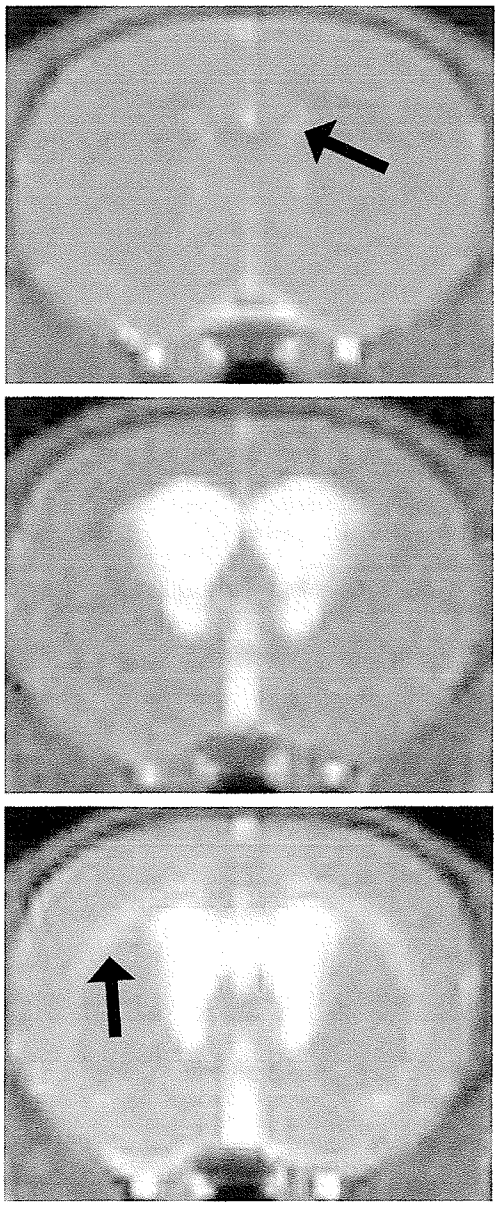

Figure 1: T2-weighted magnetic resonance images showing coronal slices through 5-week-old rat brain at the level of the anterior third ventricle. Cerebrospinal fluid (CSF) is bright. In normal rats (and induction failures) the ventricles are barely visible (upper panel; arrow). Kaolin injected at age 3 weeks is associated with marked enlargement of the lateral and third ventricles (middle panel; in this example the ventricle size index is 0.15). Other agents were less reliable. Matrigel caused moderate enlargement (lower panel; in this example the ventricle size index is 0.06). White matter edema is also apparent (arrow); it is usually associated with active enlargement.

Histological results

There were major differences between groups with respect to the histological changes in the vicinity of the cisterna magna injection sites. Kaolin along the ventral surface of the brainstem was associated with mild accumulations of neutrophils, lymphocytes, monocytes and rare eosinophils within 2d of injection (Figure 2). By 5d, collagen deposition was apparent and kaolin had clearly been ingested by macrophages. There were minimal neutrophils and eosinophils by 10d. The brainstem and cerebellum adjacent to kaolin collections were histologically unaltered. Collagen injections resulted in no evidence of inflammation and no degree of ventriculomegaly was detected at 14d (not shown).

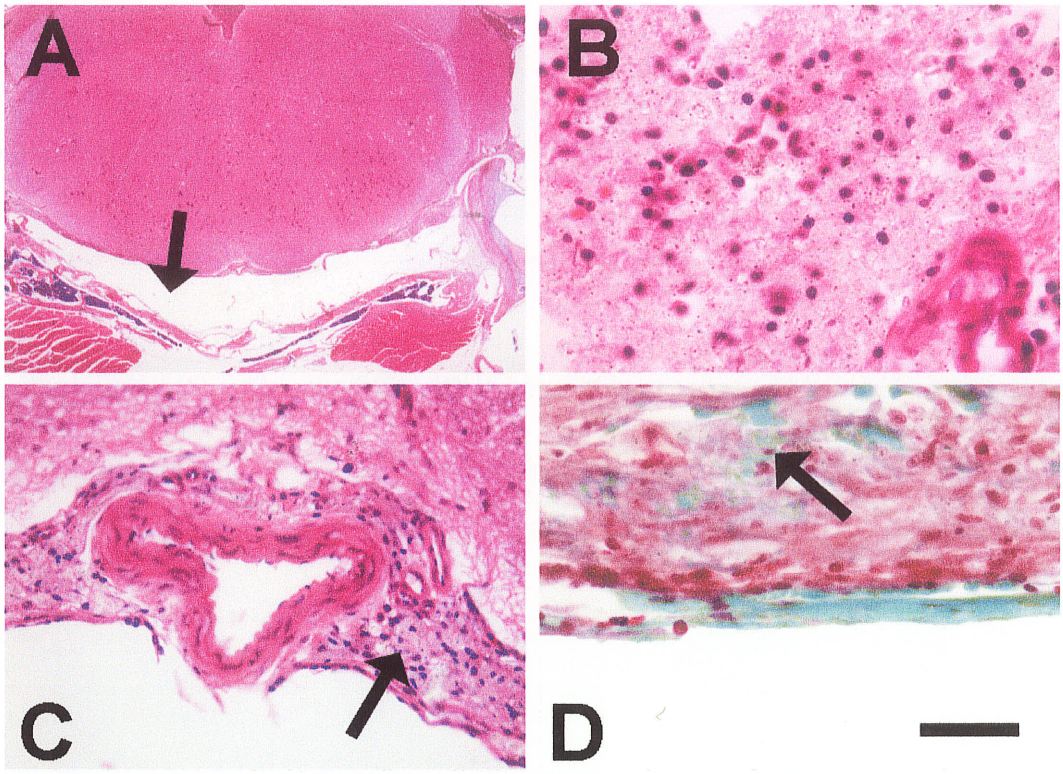

Figure 2: Photomicrographs showing effects of kaolin injection. The subarachnoid space ventral to the medulla is expanded (arrow in A; H&E stain) by aggregates of inflammatory cells and kaolin (dark granules) (B; H&E stain). Fourteen days post-injection (C; H&E stain), the kaolin has been engulfed by macrophages in the subarachnoid space (arrow); there is no abnormality apparent in the adjacent medulla. There is also arachnoid fibrosis (D; Masson's Trichrome stain) with green stained collagen (arrow) in the midst of the macrophages. Scale Bar (shown in frame D) is 50μm for B and D, 100μm for C, and 1600μm for A.

Matrigel injections were associated with increased neutrophils and lymphocytes, albeit to a lesser extent than kaolin, most likely due to the needle insertion. The Matrigel polymer appeared as an acellular homogenous faintly eosinophilic material in the subarachnoid space (Figure 3A). Matrigel spread well beyond the brainstem into some of the cerebellar sulci. It appeared to be surrounded by fibroblasts and hyperplastic small blood vessels with mild collagen accumulation at 5d. From 5-14d there was no evidence of vascular growth into the gel mass and there was no inflammation (Figure 3B). In one animal, the injection site was missed and the Matrigel was injected into the cerebellum. This resulted in a normal MR image with no enlargement of ventricles and normal weight gain and behavior.

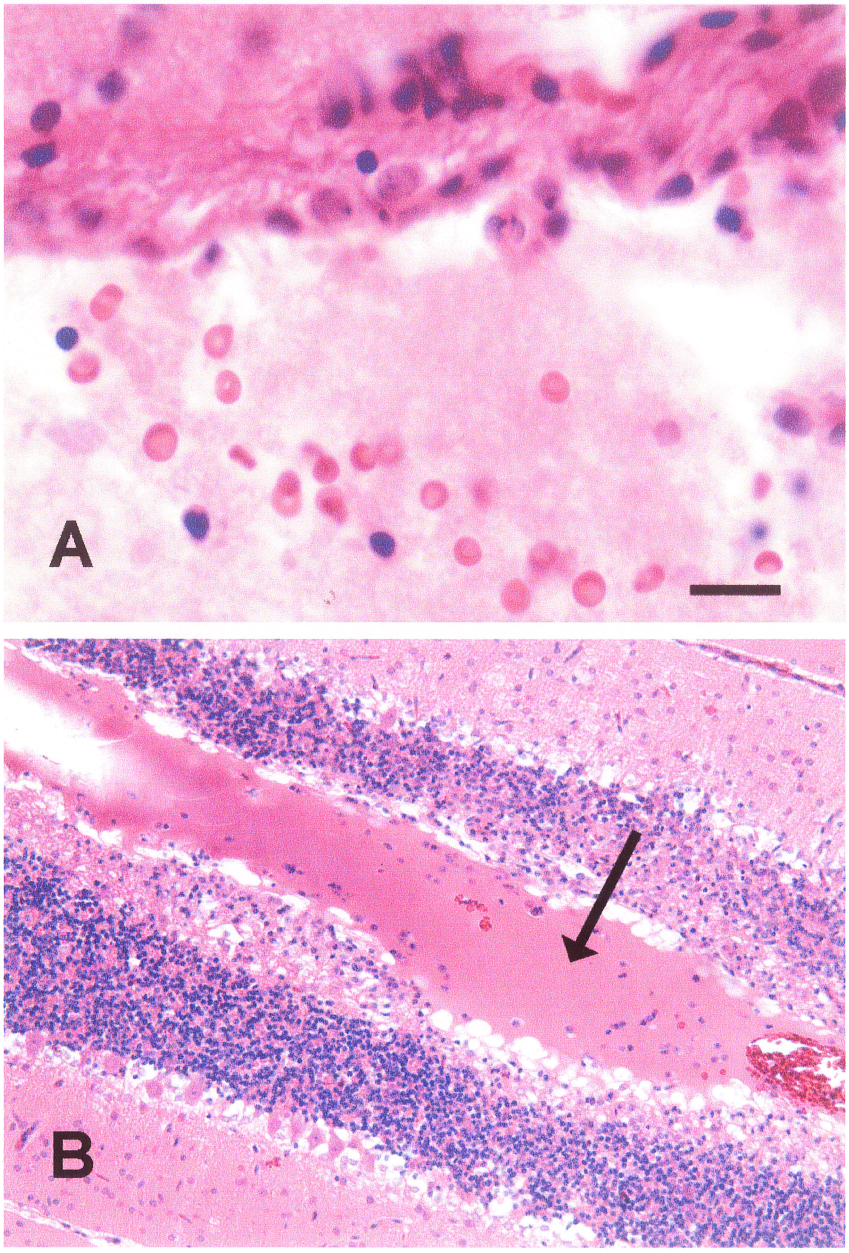

Figure 3: Photomicrographs showing effects of Matrigel injection. Two days post-injection (A; H&E stain) the ventral subarachnoid space is filled with Matrigel, which appears as an amorphous protein gel with scattered blood cells. Five to 14d post-injection (B; H&E stain), the Matrigel spreads around the cerebellum and into sulci (arrow) forming an acellular mass that does not elicit an inflammatory response but traps some of the blood cells. Scale Bar (shown in frame A) is 25μm for A and 100μm for B.

Ethylene vinyl polymer appeared as a transparent material with black granules (tantalum) located in the fourth ventricle and lateral subarachnoid space (Figure 4A). Unlike kaolin and the proteins, it is viscous and does not spread into the ventral subarachnoid space. Arachnoid fibrosis and severe inflammatory responses (neutrophils and multinucleated foreign-body giant cells) were apparent at 2d post-injection (Figure 4B). At 5d there was an increase in the number of giant cells present, minimal neutrophils, and early collagen formation (Figure 4D). These changes persisted at 14d (Figure 4C).

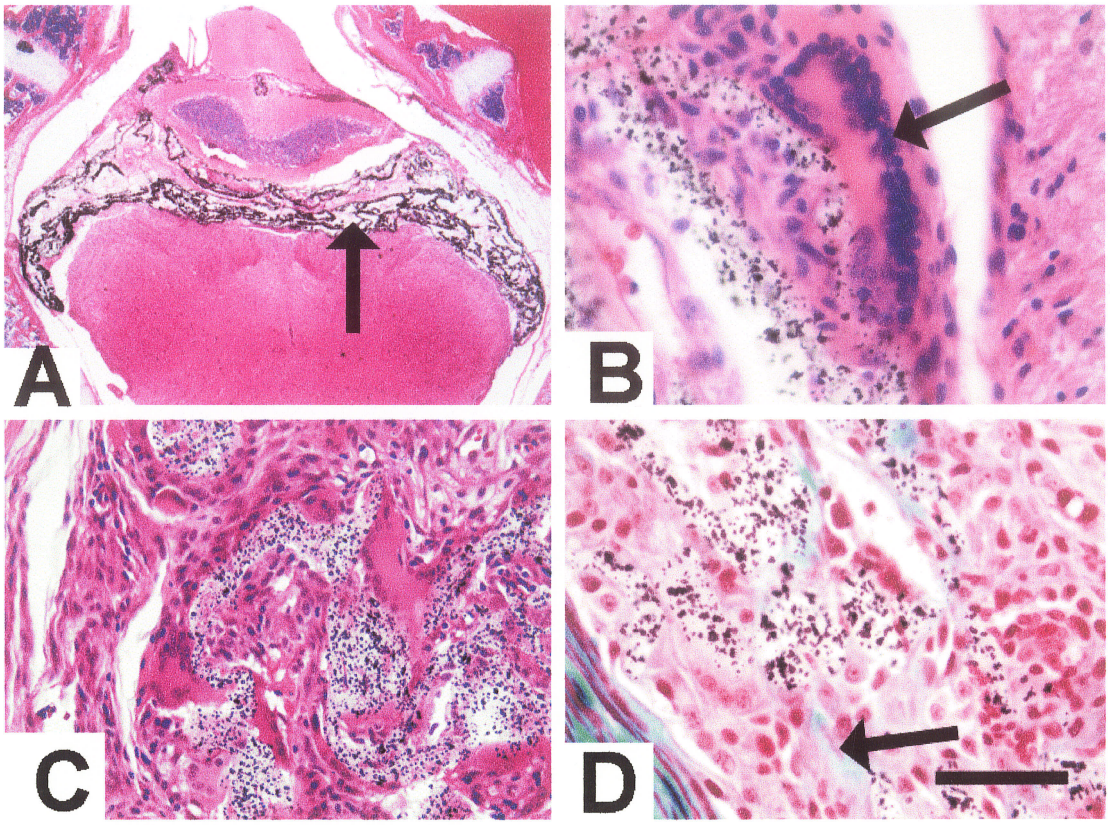

Figure 4: Photomicrographs showing effect of ethylene vinyl alcohol copolymer (Onyx) injection. At low magnification (A; H&E stain), the black tantalum granules in the polymer matrix are obvious in the fourth ventricle (arrow). By 2d (B; H&E stain) multinucleate (foreign body reaction) giant cells are apparent (arrow) adjacent to the Onyx. By 14d (C; H&E stain) the giant cell and fibroblastic reaction is more advanced, surrounding the Onyx clusters. There is associated collagen (green material, arrow) deposition as early as 5d (D; Masson's trichrome stain). Scale Bar (shown in frame D) is 50μm for B and D, 100μm for C, and 1600μm for A.

Histological analysis of fibrin glue and NBCA was only done at 14d because it had become quickly apparent that there was no successful induction of hydrocephalus. NBCA caused moderate arachnoid cell proliferation without evidence of inflammation (not shown). In the present experiment, fibrin glue caused moderate arachnoid cell proliferation but only mild inflammation at 14 days post-injection.

Discussion

Kaolin injection is an effective method for producing hydrocephalus in almost all animal species tested [103]. Although this method offers dose-dependent responses to some extent, the response is variable. The inflammatory response consisting largely of macrophages with some lymphocytes that results in obstruction to CSF flow, is a potentially confounding factor. Although it is an aluminum-based compound, in rats surviving 9 months after kaolin injection there is no evidence that the material spreads very far, nor is there an association in this model with formation of neurofibrillary tangles (Del Bigio; unpublished observations 2003). Injectable polymerizing agents, both protein based and synthetic, appeared to offer an effective alternative to kaolin because they solidify into a gel matrix that may conform to the subarachnoid compartment. The proteins Matrigel, collagen I, and fibrin have all been reported to support cell survival, growth and angiogenesis in cardiac muscle [157].

Collagen I is the most abundant extracellular matrix protein [158]. It is found in most tissues and organs, including dermis, tendon, cartilage, ligaments and bone. A

significant proportion of the extracellular matrix of the leptomeninges is also composed of collagen [159, 160]. It has great tensile strength and gives support and structure to cells of the extracellular matrix. It can be used as a thin layer on tissue-culture surfaces to enhance cell attachment and proliferation, or in vitro as a gel to promote expression of cell-specific morphology and function [145, 157]. Type 1 collagen is commonly used to culture endothelial cells, hepatocytes, muscle cells, and a variety of other cell types. The high protein concentration results in a sturdier gel which provides maximal support to maintain the 3D environment [161, 162]. In this experiment, we expected collagen I to form a protein plug when injected into the cisterna magna of rats with minimal inflammatory response. Preliminary experiments of applying the collagen to a glass slide resulted in formation of a solid protein gel. When injected into the cisterna magna of rats we found that collagen was entirely ineffective at producing ventriculomegaly. Subsequent experiments demonstrated that collagen dissolved immediately when injected into artificial CSF.

Our most promising compound was Matrigel. The main components of Matrigel are structural proteins such as laminin (61%) and collagen IV (30%). This mixture resembles the complex extracellular environment found in many tissues and is typically used by cell biologists as a substrate for cell culture. Matrigel is stored at -20°C and thaws to liquid consistency at 10°C, which makes it very easy to work with at room temperature. At 37°C it self-assembles into a gel. When injected into the cisterna magna, Matrigel spread locally in the subarachnoid compartment forming protein casts thereby retarding CSF flow and producing mild ventriculomegaly. Matrigel associated-hydrocephalus caused no inflammation beyond that associated with the needle insertion.

However, we could not attain the magnitude of ventriculomegaly possible with kaolin. Furthermore, in the course of the experiment we noticed differences between batches of Matrigel purchased from the supplier; one batch was less viscous than the first and larger volumes were required. One would need to address issues of initial protein concentration to avoid large injection volumes. It remains to be determined if the effect would be stable. It has been suggested that Matrigel, collagen I, and fibrin might be absorbed after ~5 weeks [157].

Fibrin glue is a widely used surgical tissue adhesive used to control bleeding and block CSF leaks [155]. In experimental application to brain surface it causes an inflammatory reaction that peaks at ~1 week and persists with lymphocytes and foreign body giant cells for weeks [163, 164]. It appears to be relatively non-reactive with neural tissues, stable in CSF and resilient to natural degradation in the sub-arachnoid space [155, 156]. It is a viscous solution that adheres to wound surfaces and quickly sets to form a rubber-like mass for the purpose of sealing or gluing tissues. It is a two-component solution composed of a highly concentrated fibrinogen and aproptonin mixture, and a separate solution of thrombin and calcium chloride. All 4 of these additives came separate from the supplier, and required combining in 2 separate needles prior to administration. Two concentrations of thrombin (4 IU/mL and 500 IU/mL) were also given by the supplier to control the setting rate of the sealant. The setting process will be complete within 1 minute with the 4 IU/mL thrombin concentration, while the 500 IU/mL concentration sets in seconds. Initial *in vitro* experiments with the two thrombin concentrations showed no real difference in the setting rate of either solution, as both were completely set within 10 seconds when injected into artificial CSF. The fibrin glue

proved to be extremely difficult to administer and provided significant limitations to its application in this experiment. The dual applicator jet provided by the manufacturer was large and bulky and hindered our ability to accurately place the needle in the cisterna magna. Due its high viscosity, it was also extremely difficult to administer through a fine needle. Other difficulties included the fact that the thrombin solution had to be kept at 37°C until immediately before use. In addition, the compounds would solidify immediately on contact and thus clog the applicator or form a bulky mass in the cisterna magna, compressing the brainstem and resulting in acute death. It is also noted by the supplier that the rubber-like mass which forms, continues to gain strength for 2 hours following its application, which may have contributed to our high rate of acute death in these rats.

The two synthetic agents tested, N-butyl-cyanoacrylate (NBCA) and ethylene vinyl alcohol copolymer (Onyx), were unacceptable for different reasons. NBCA is a rapidly polymerizing agent that adheres to vessel walls and surrounding tissue [149]. The chronic local tissue irritation and inflammation associated with cyanoacrylates is related to the degradation products of the polymer, which include formaldehyde and alkyl cyanoacetate [165, 166]. Although NBCA has been useful for production of hydrocephalus in dogs, the jagged edges of the hardened adhesive found adjacent to the brainstem proved fatal for largely mechanical reasons. Polyvinyl alcohols are also used for endovascular embolism treatments. Unlike NBCA, they are non-adhesive and flexible, and produce less inflammation [166]. The use of the ethylene vinyl alcohol copolymer (Onyx®) was successful in producing moderate hydrocephalus, but induced a severe inflammatory reaction. This included severe arachnoid fibrosis and the invasion of

neutrophils, macrophages, and lymphocytes. We also observed intense foreign body giant cell type reaction in response to Onyx, by 2 days post-injection, consistent with the reported vascular responses [167-169]. It has been suggested that DMSO can cause severe inflammation following intra-arterial injection [151], however, DMSO has also been used as an anti-inflammatory agent [170].

The age of the rats used should be considered. In our experience with rats ranging from newborn to adult there is little variation with respect to the response to kaolin, although other species such as sheep exhibit more lymphocytic response to kaolin (unpublished data). We expect that adult rats would respond in a similar manner and that younger rats might suffer more serious complications with the rapidly hardening agents because their fourth ventricle and cisterna magna are smaller.

Conclusions

The objective of this study was to establish a non-inflammatory model of hydrocephalus in rats, using alternative protein and synthetic biopolymers. We hypothesized that at least one of the agents tested would be as efficacious as kaolin for induction of hydrocephalus in young rats. The injection of kaolin into the cisterna magna predictably results in an inflammatory fibrosis of the meninges and an obstruction of the fourth ventricle outlets, thus leading to the development of hydrocephalus. Injectable polymerizing agents, both protein-based and synthetic, appeared to offer an effective alternative to kaolin because they solidify into a gel matrix that could conform to the subarachnoid compartment. The natural polymers offered minimal inflammation but

resulted in too much dispersion in the subarachnoid space. The synthetic polymers were more stable in the subarachnoid space, however they resulted in severe inflammation and significant local tissue damage as well as brain stem compression. Although we were successful in inducing hydrocephalus through cisternal injections with Matrigel and ethylene vinyl alcohol copolymers, neither of these biopolymers was as reliable as kaolin. Based on our observations, we conclude that none of the agents tested are better than kaolin for use in rats. Further study of the Matrigel protein polymer is warranted, as it proved easy to work with and was associated with only mild ventriculomegaly and minimal inflammation. However, until efficacy can be shown, we plan to continue use of kaolin, which reliably and inexpensively produces severe ventriculomegaly in experimental animals. The caveat is that one must be willing to accept the remote possibility that the inflammation is a confounding factor in hydrocephalus-induced brain damage.

Chapter 3: Use of kaolin injection method to induce hydrocephalus in mice

Abstract

Background: Kaolin has been used successfully to induce hydrocephalus in many species, but seldom in mice. The purpose of this study is to produce hydrocephalus in mice by the injection of kaolin into the subarachnoid space at the cisterna magna.

Methods: Kaolin was injected into the subarachnoid space at the cisterna magna of 35 adult CD1 mice, while 9 controls received a sham sterile saline injection. This method was repeated with thirty-four 7-day old mice, and 10 controls received a sham saline injection.

Results: Twenty adult animals and 5 juvenile mice experienced acute distress and died immediately upon injection. Assessment of hydrocephalus in surviving animals was performed by magnetic resonance imaging on days 7, 14, 21 or 30 post-injection or before each animal was to be euthanized if it fell outside of the predetermined days. All 15 surviving adult mice and 22 out of 29 surviving injected juveniles exhibited altered signal in the vicinity of the ventricles, which is consistent with the development of hydrocephalus. Microscopic examination showed enlarged ventricles in all mice with altered MR signal.

Conclusions: Acute complications of the injection are high because the cisterna magna of mice is extremely small and brainstem injury possible. However when carefully administered, kaolin can successfully be used to induce hydrocephalus in both adult and young CD1 mice.

Background

Experimental hydrocephalus can be induced by injection of kaolin (aluminum silicate) into the cisterna magna [134]. Ventricular enlargement occurs as a result of the inflammatory scarring, which causes an obstruction of the cerebrospinal fluid (CSF) pathways at the fourth ventricle outlets. This model has been used in a wide range of species including rats, guinea pigs, rabbits, cats, dogs, sheep and primates [103]. The use of mice in the study of experimental hydrocephalus has mainly been accomplished through use of transgenic/knockout animals [171, 172]. Until recently, there has been no literature concerning the use of mice in a mechanical model of hydrocephalus.

In 2006 there were two papers published both claiming successful induction of hydrocephalus in adult mice using an open incision method and injection of kaolin into the cisterna magna [138, 139]. Hatta et al (2006) reported success with 2μL of 2% kaolin injected into the cisterna magna through the atlanto-occipital membrane of 10-12 week old Jcl:ICR mice. However, they failed to document number of animals used nor did they mention the success rates of their injections. Bloch et al (2006) used aquaporin null mice and controls on a CD1 strain and reported an 80% survival rate when a 1cm midline vertical incision was made over the back of the neck from the top of the occiput to C1 to allow injection of 10μL of 25% kaolin. Their group sizes are substantial (30 and 33 respectively) and they report a mild but significant increase in ventricle size based on histological examination at 5 days. However they noted that their animals experienced a rapid decline in health after day 5. Although both of these papers reported successful induction of hydrocephalus in mice, their method of induction is difficult to administer

and an easier method should still be investigated. Our laboratory has had great success with the (closed) cisterna magna injection method in a variety of species, although we have not attempted this procedure with mice.

The purpose of the present experiment is to produce a hydrocephalus model in adult and young mice by percutaneous (closed) kaolin injection into the cisterna magna. Such a simple model would be useful because mice with genetic mutations could then be used to test the role of various proteins in the pathogenesis of hydrocephalic brain damage.

Materials and Methods

All animals were locally bred CD1 male mice. All were treated in accordance with the guidelines of the Canadian Council on Animal Care and protocols were approved by the institutional animal ethics committee. Humane endpoints for euthanasia were established prior to experimentation to avoid unnecessary suffering, such as reduced mobility, respiratory distress and severe neurological impairment.

Four groups of 11 mature 6-8 week-old CD1 mice, as well as 4 groups of 11 seven-day old CD1 mice were used for this study. Mice were anesthetized and maintained with isoflurane gas (1.5% in oxygen). The head and neck were shaved and cleaned with Hibitane. Mice were placed head down on a raised platform with the neck flexed to maximize exposure to the foramen magnum. Under aseptic conditions, a 0.30 ml syringe with 30-gauge needle was used for injection of sterile kaolin suspension

(aluminum silicate; Sigma, St. Louis MO) (100-250mg/ml in 0.9% saline). Animals were monitored during recovery from anesthetic, weighed daily and observed for signs of neurological impairment. Adult mice were housed 5 to a cage and allowed food and water freely. Young mice were placed back in the cage with their mother until they reached appropriate age for weaning.

From each group of adult mice, 8-9 were injected with kaolin and 2 controls received the same volume of sterile saline. From the 4 groups of 7-day old mice, ~9 received kaolin while 1 or 2 controls received the same saline control injection. The injected volumes were initially arbitrarily chosen based on our previous experience with rats of similar size and weights. We injected the first two batches of mice (adults and juveniles) with 25% kaolin, (25μL and 10μL respectively). We noted a rapid decline in the overall health of these animals around day 5. We subsequently injected the third batch of animals with 20% kaolin (10μL and 5μL respectively) and the final batch of animals with 10% kaolin (10μL and 5μL respectively). We progressively altered the kaolin concentration based on a hypothesis that a less viscous solution would allow better spread of the kaolin and therefore result in a lesser degree of brain stem compression.

Magnetic Resonance Imaging

Magnetic resonance (MR) studies were performed using a Bruker Biospec/3 MR scanner equipped with a 21-cm bore magnet operating at a field of 7 T (Karlsruhe, Germany) to obtain T2-weighted images of the brain in the coronal, horizontal, and sagittal planes. The mice were anesthetized briefly with 1.5–2% isoflurane. These

methods have been previously described in detail [152]. Mice underwent MR imaging once humane endpoints had been reached or after 7 or 14 days post-injection as previously predetermined.

Behavior Testing

On alternating days beginning on post-injection day 2, all mice were observed in an open field situation for a period of 1 min to assess arousal, grooming, and gait by using a previously validated set of parameters [173-175]. Quantitative monitoring of spontaneous activity was then performed for 9 minutes in a square enclosure (43 x 43 cm) with 15 infrared beams (spaced every 3 cm) along the floor in each of two horizontal directions and a third set of similarly spaced beams 6.0 cm above the floor (Opto-Varimex; Columbus Instruments, Columbus OH, U.S.A.). Vertical, total, and ambulatory beam breaks were counted, the latter being defined as an interruption in a series of adjacent beams.

Gait, agility and motor functions of adult mice were assessed using a rotating cylinder of 7-cm diameter in 2 separate trials (Economex, Columbus Instruments). First, endurance at a constant speed of 5.0 rpm was assessed for a maximum of 2 minutes. Second, we measured the ability to stay on the cylinder, which accelerated beginning at 5.0 rpm and increasing at a rate of 0.1 rpm every second for up to 2 minutes. The time was recorded from the moment the mouse was placed on the rotating cylinder until it fell off. The rotating cylinder test is complex and involves proprioceptive, tactile, vestibular, and motor functions. Motor coordination and balance is assessed by measuring the ability of the mice to traverse a beam, (55cm long x 4cm wide, 80cm off the ground) to reach an

enclosed safety platform. The outcome measures and testing protocols for rotating cylinder are the same as those described in juvenile rats with hydrocephalus [173, 174, 176].

Post-injection monitoring and sacrifice

Animals were monitored during recovery from anesthetic, weighed daily and observed for signs of distress and neurological impairment. Mice were euthanized immediately once signs, such as prolapsed penis, severe ataxia, severe motor dysfunction, signs of dehydration or dramatically decreased body weight were recognized. Adult mice were housed 5 to a cage, while young mice remained with their mother. All animals were allowed food and water freely. Euthanasia using carbon dioxide gas was administered after MR imaging, followed by perfusion with 0.1M phosphate buffered saline (PBS) through cardiac puncture. Brains were removed and fixed in 3% paraformaldehyde followed by paraffin embedding. Brains were then cut into 6μm sections, dewaxed and stained with hematoxylin/eosin for microscopic analysis.

Results

Mortality

A total of 44 adult mice and 44 juvenile mice were studied. Of the 35 kaolin-injected adult mice, 20 died immediately after injection (usually due to respiratory failure, or less often failure to regain consciousness). Of the 15 adult survivors, all were

euthanized between day 5 and 14 either due to signs of severe neurological deficit or the predetermined endpoint of the study was reached. Of the 34 juvenile mice injected with kaolin, 5 died immediately after injection, and survivors were euthanized between days 2 and 14 for the same reasons. Figure 5 demonstrates a Kaplan-Meier survival plot for mice of each age group.

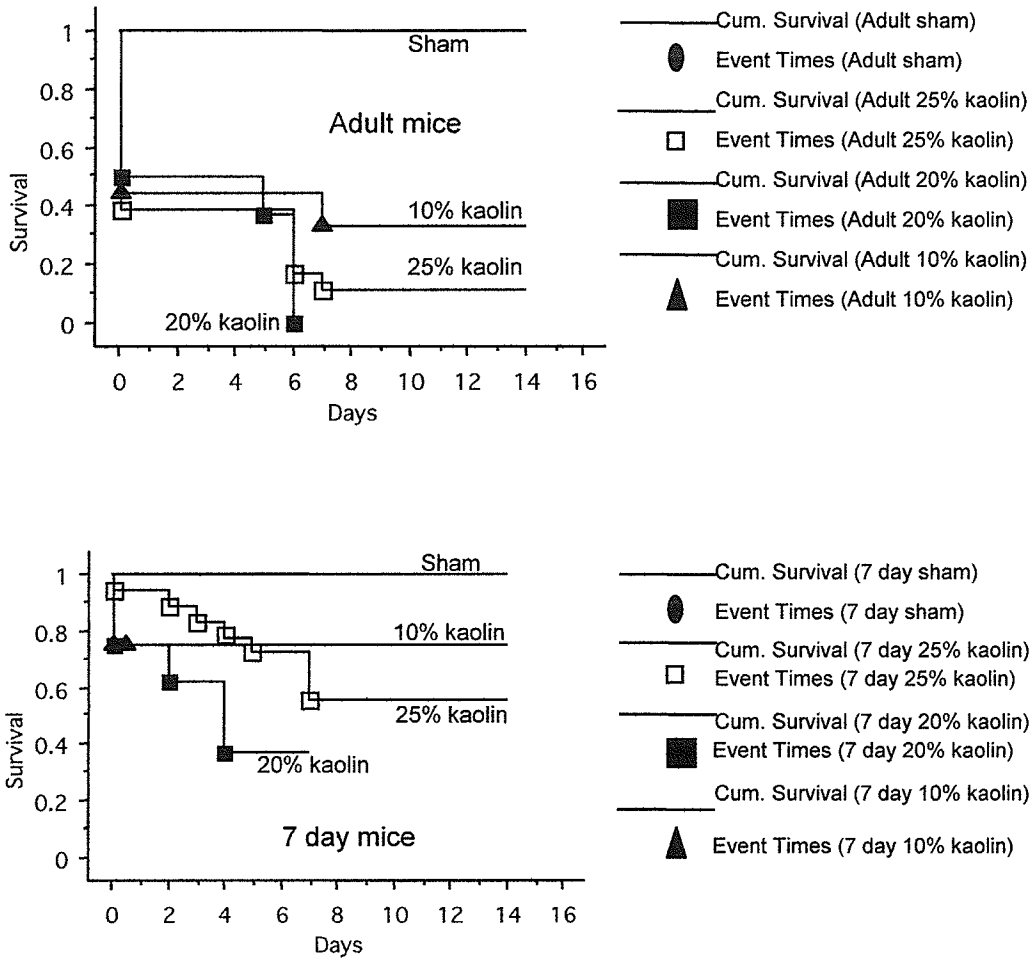

Figure 5: Kaplan-Meier survival plot for day of death for adult and juvenile mice.

Behavior

Juvenile hydrocephalic mice exhibited a significant lag in weight gain and adult hydrocephalic mice lost weight in comparison to controls, as shown in Figure 6. Hydrocephalic animals had an abnormal broad-based stance with tiptoed stepping and a hunched back. However, the results of the open field investigation showed that an animal's behavior score did not change significantly with disease progression until there was a very rapid decline immediately before euthanasia was mandated. It was anticipated that the 9 minute activity monitoring might reveal some differences. However, in no group did the results show a tendency to habituation and therefore cumulative scores for vertical exploration and ambulation were analyzed. Both adult and juvenile hydrocephalic mice showed no differences in ambulatory or vertical activity at 7 or 14 days post injection compared to age-matched controls, as shown in figure 7 and in table 2. We also found that the juvenile mice were too small at 14 days old to break the vertical beams, therefore we cannot consider this data to be very reliable at such a young age. In tests of motor function, hydrocephalic mice failed to show any differences from controls; all mice remained on the constant speed and accelerating rotorod for 2 minutes without falling. The beam walking test also failed to discriminate between control to hydrocephalics; all animals crossed the beam within 5-10 seconds without falling.

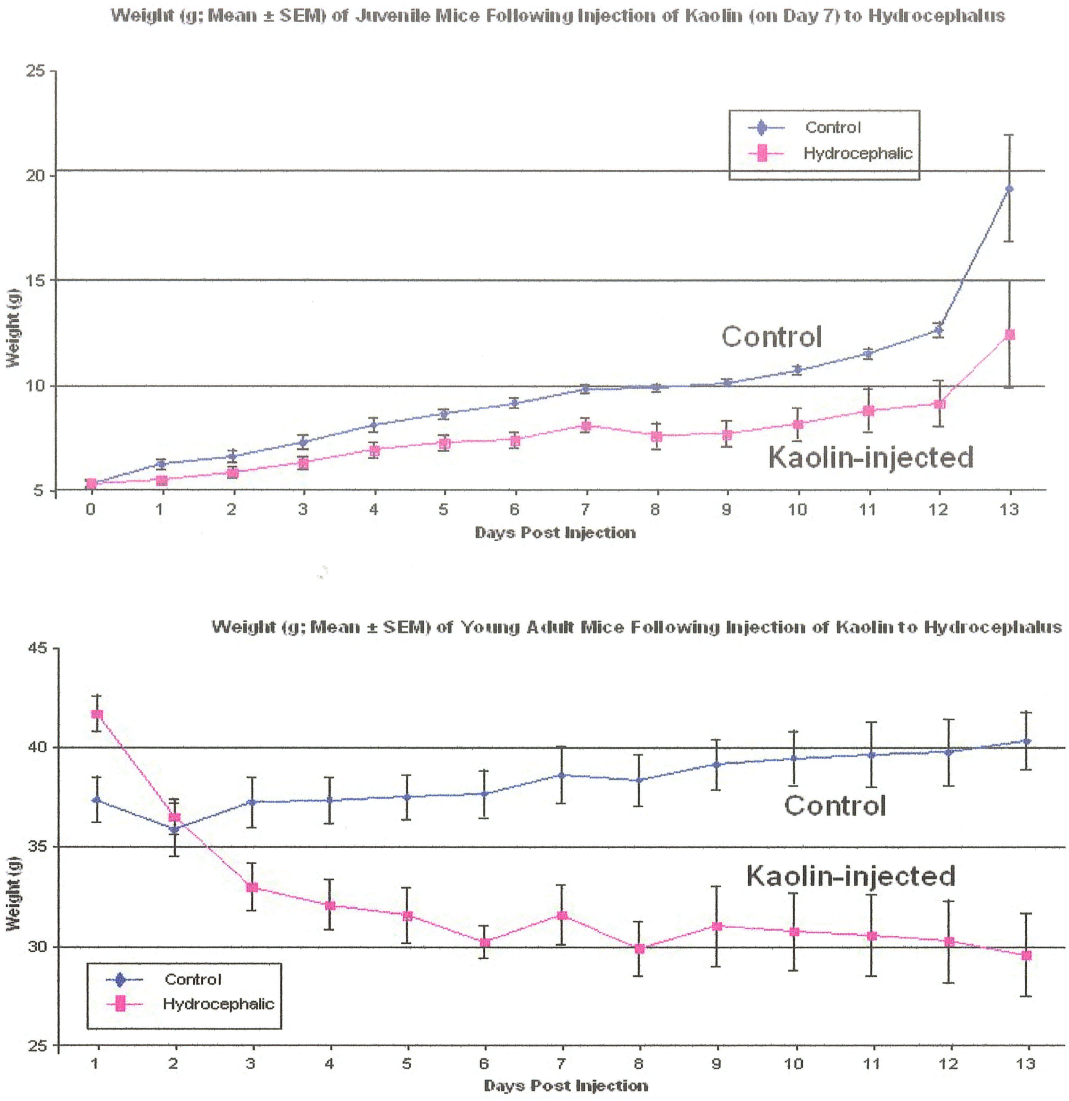

Figure 6: Line graphs showing daily weights (grams) of control (diamond) and hydrocephalic (square) mice (mean ± SEM). Juvenile mice in top panel and adult mice in bottom panel. The hydrocephalic mice displayed a significantly lower body weights by 14 days post-kaolin injection when compared to controls.

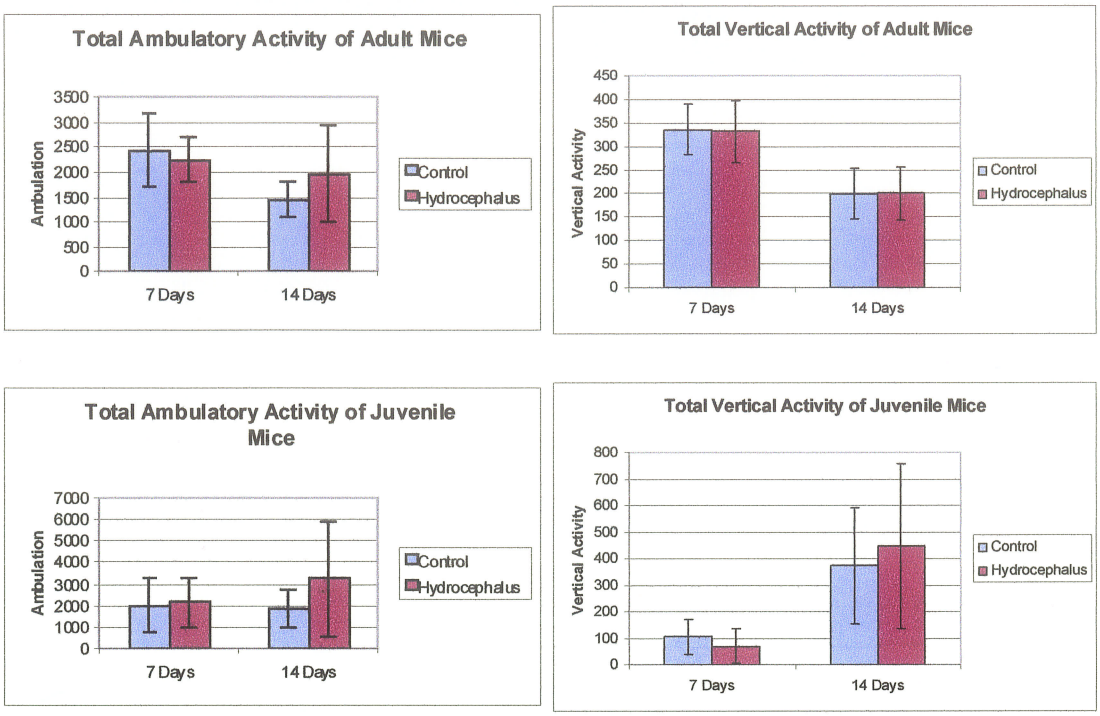

Figure 7: Bar graphs showing cumulative activity of adult and juvenile mice at 7 and 14 days post injection. Top panels show total ambulatory activity rates (Mean±SEM) and bottom panels show vertical activity rates (Mean ± SEM)

	Total Ambulatory Activity of Mice					
	7 Days			14 Days		
	Mean	SEM	p	Mean	SEM	p
Adult Control	2434.50	738.72	0.67	1451.00	355.59	0.44
Adult Hydrocephalic	2253.83	445.00		1969.50	969.43	
Juvenile Control	2020.57	1269.14	0.87	1871.00	864.58	0.36
Juvenile Hydrocephalic	2166.20	1164.97		3267.00	2654.99	

	Total Vertical Activity of Mice					
	7 Days			14 Days		
	Mean	SEM	p	Mean	SEM	p
Adult Control	336.00	54.09	0.93	199.25	54.05	0.97
Adult Hydrocephalic	331.67	66.30		201.00	56.20	
Juvenile Control	104.57	66.92	0.48	373.50	219.57	0.72
Juvenile Hydrocephalic	69.40	64.78		446.25	312.08	

Table 2: Total ambulatory and vertical activity of adult and juvenile control and hydrocephalic mice at 7 and 14 days post-injection. T-tests conducted on adults and juveniles show no significant differences between control and hydrocephalic mice in either age group.

Hydrocephalus induction

All 15 kaolin-injected adult mice and 22 out of 29 kaolin-injected juvenile mice exhibited periventricular bright signal on the T2-weighted MR images, representing enlarged ventricles and/or increased water in the vicinity of the ventricles (Figure 8). The bright signal was evident at 2 days post-injection in both ages. The ventricle sizes are summarized in Table 3. Ventricular enlargement was associated with a dome-shaped head and/or persistent fontanel, which could be seen as early as 4 days post-injection. This aspect was far more obvious in the young mice (Figure 9).

Age	Kaolin %	Mean Ratio±SEM	Range
Adult +7d	25	0.121±0.020	0.088 to 0.176
Adult +6d	20	0.127±0.009	0.118 to 0.135
Adult +14d	10	0.240±0.036	0.135 to 0.291
7 +7d	20	0.432±0.050	0.338 to 0.507
7 +14d	10	0.522±0.110	0.259 to 0.761

Table 3: Calculated ventricle-brain ratios for adult and juvenile mice at selected time points.

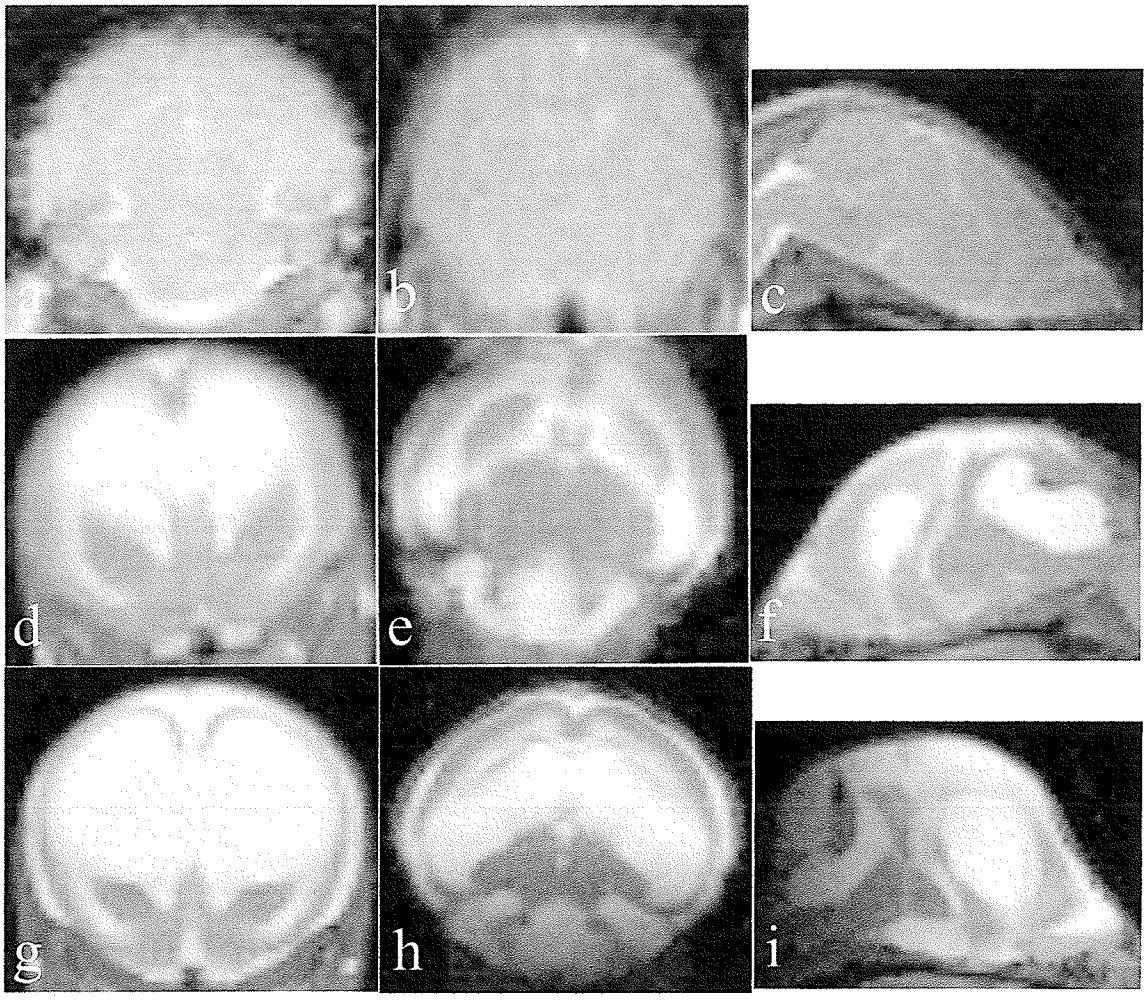

Figure 8: T2-weighted magnetic resonance images showing coronal (left column), horizontal (middle column) and sagittal (right column) slices through juvenile mouse brains. Juvenile control brain at 14 days post saline injection with calculated ventricular dilatation of 0.01 (a, b, c). Hydrocephalic mouse brain 7 days post kaolin (10%) injection with calculated ventricular dilatation of 0.42 (d, e, f). Hydrocephalic mouse brain 14 days post kaolin (10%) injection with calculated ventricular dilatation of 0.65 (g, h, i).

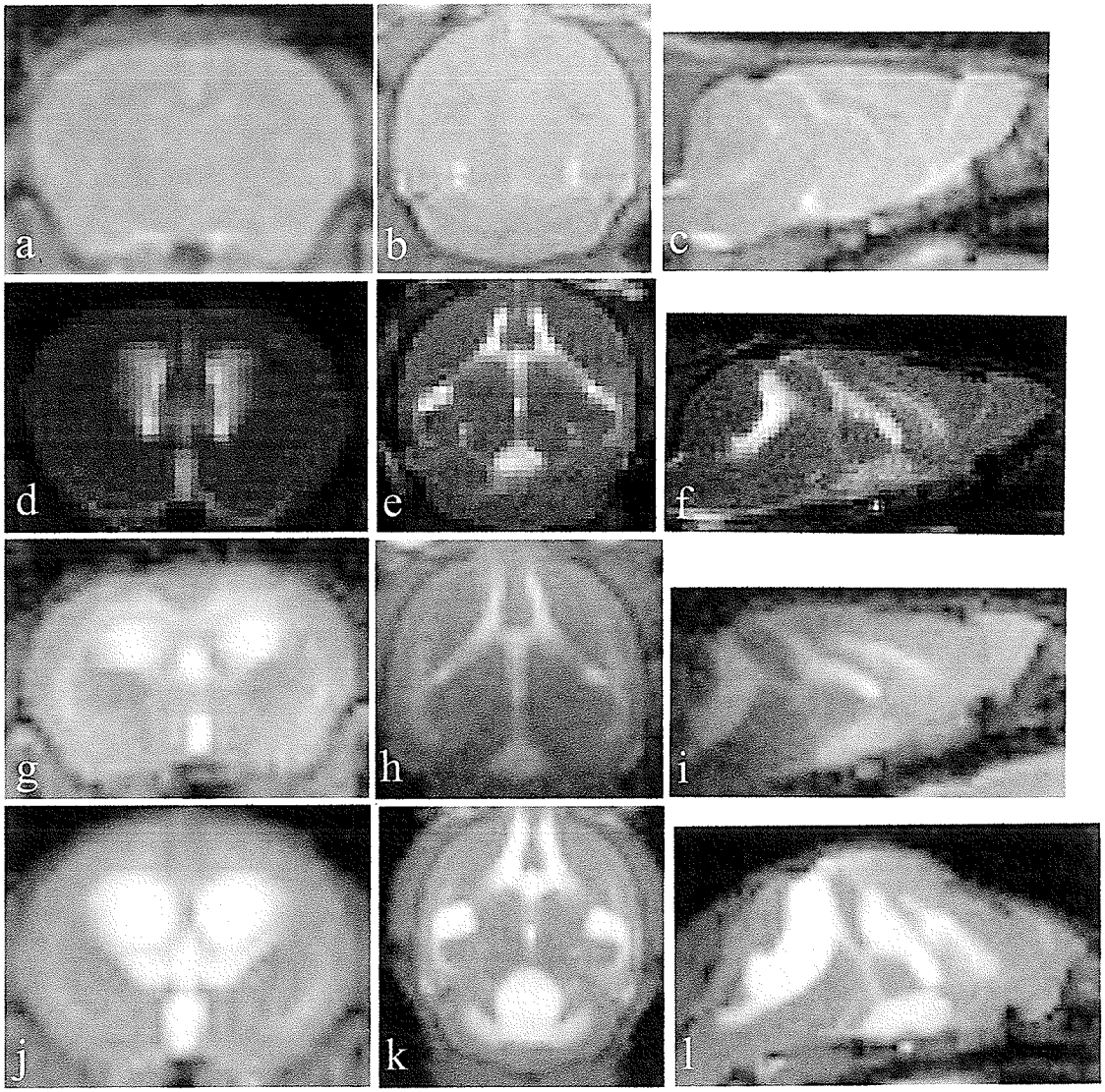

Figure 9 : T2-weighted magnetic resonance images showing coronal (left column), horizontal (middle column) and sagittal (right column) planes through adult mouse brains. Control brain at 14 days post-saline injection with calculated ventricular dilatation of 0.001 (a, b, c). Adult brain 7 days post kaolin (25%) injection (d, e, f) showing positive bright signal intensity in the ventricular region. Microscopic examination showed no ventricular dilation, indicating that this represents only edematous surrounding tissue. Adult brain 7 days post kaolin (10%) injection with calculated ventricular dilation of 0.14 (g, h, i). Adult hydrocephalic brain at 14 days post kaolin (10%) injection with calculated ventricular dilatation of 0.28 (j, k, l).

Microscopy

Upon microscopic examination there was definite evidence of ventricular dilation in all juveniles and adult mice with enhanced MR signal. In all of the juvenile kaolin-injected mice that did not develop hydrocephalus, a dark spot in the cerebellum was evident on the MR, representing a missed injection site, characterized by either hemosiderin or a kaolin deposit. All hydrocephalic brains displayed enlarged ventricles with normal appearing choroid plexus and an intact ependymal lining. The periventricular tissue was of normal density in the majority of mice, both adults and juveniles, with the exception of the most severely hydrocephalic brains, demonstrating mildly loose and edematous periventricular tissue, specifically along the roof of the dorsolateral angle of the lateral ventricles (Figure 10). In cases of severe hydrocephalus, the thickness of the cortex and corpus callosum was drastically reduced. Control mice displayed small fused ventricles with periventricular tissue of normal density.

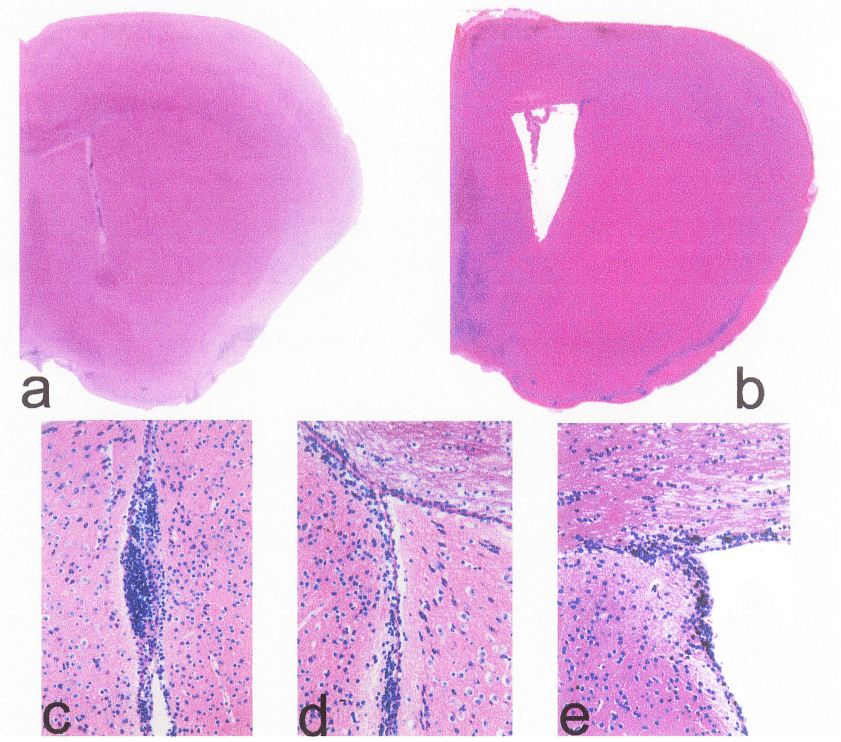

Figure 10: Photomicrographs of adult mouse brains 14 days post kaolin injection: Coronal slices of lateral ventricles stained with hematoxylin and eosin. Sections demonstrate fused/normal lateral ventricles at low (a) and high magnification (c) in control mice. Normal ventricles with loose and edematous surrounding tissue (d) corresponds to bright signal intensity as seen on MR analysis in Figure 7 (d, e, f). Enlarged ventricles with intact ependyma in (b) and (e) demonstrate mild to moderate hydrocephalus, which corresponds with bright signal intensity seen on MR images in Figure 7 (g, h, i). Magnification: 12.5x (a, b), 40x (c, d, e).

Discussion

Despite substantial experience with the kaolin model in a wide range of species in our laboratory, we experienced some difficulty in our first attempts with mice. Previously this method had been attempted by another member of our laboratory, utilizing the percutaneous injection method as well as the open cisternal injection. The injections of kaolin had been associated with over 90 % mortality rate and a low success rate in creating ventriculomegaly. Although many mice had enhanced signal in the region of the ventricles on the MR imaging associated with an elevated ICP, the ventricles were seldom dilated when examined histologically. In apparent successes, defined by neurological impairment, changes on MRI and raised ICP (data not shown), there was no ventricular enlargement on microscopic examination. In fact the ventricles were found to be fused in some areas as shown in Figure 10. These observations are consistent with those made by Westergard [178] and Sturrock [179]. Coarctation is found in the anterior portion of the anterior horn, the inferior portion of the inferior horn, as well as in the posterior of the inferior horn in 96.4% of full-grown AK/a inbred albino mice but is absent in the newborn [178]. The fusions develop in the mouse embryonic state and continue to develop according to a definite pattern, occurring symmetrically in the lateral ventricles [178]. We suggest that the increase in pressure without ventricular enlargement may in fact resemble pseudotumor cerebri, rather than acute hydrocephalus.

The open incision method used to induce hydrocephalus described by Hatta et al (2006) and Bloch et al (2006) is complex and time consuming. We have attempted to duplicate this method in our laboratory without success, although Bloch et al. reports >80% survival using this procedure. Bloch et al. (2006) also reports a rapid decline in the

health of the hydrocephalic mice at 5-7 days post injection [138]. This may be directly related to the high concentration of kaolin that was used. As the fibrosis of the meninges at the cisterna magna progresses, there is a reduction in communication between the ventricular and extra-ventricular CSF compartments with restricted flow into the cranial subarachnoid space. This lack of CSF drainage and absorption after 5 days may be directly related to the severity of the fibrosis seen at the cisterna magna resulting from 25% kaolin, thus leading to brainstem compression.

Hatta et al.(2006) reports successful induction of hydrocephalus in adult mice at 8-10 weeks of age, using only 5μL of 2% kaolin suspension in distilled water [139]. Although their group size is very small and their mortality rate is not reported, they describe that 5 mice survive to day 14 and that 1 animal survives through to day 28 post-injection. They also show a mild to moderate degree of ventriculomegaly in their figure 2. Based on the inconsistencies of these two reports, we decided to verify the findings and get better characterization of the model. In the present study, the cisternal injections of kaolin were associated with 57 % mortality rate in the adult mice and 15% in juveniles. Acute complications including a high mortality rate related to cisterna magna injections are likely because mice have a very small 4^{th} ventricle and a tight posterior fossa. This is readily apparent on the MR images where no CSF is visible in the fourth ventricle of normal mice (Figure 7). This presents difficulty in administering a sufficient amount of kaolin for the induction of hydrocephalus without causing acute injury to the brainstem. In apparent successes, defined by decreased weight gain, neurological impairment and changes on MRI there was sufficient ventricular dilation upon microscopic examination.

Motor activity underlies almost every behavioral paradigm [177]. For most behavioral pattern modeling, animals have to be adult (at least 70 days of age) in order to obtain reproducible results, as testing animals younger than 70 days may give results that are influenced by their development [180]. Based on rat and mouse behavior literature, we hypothesized that there would be differences in motor coordination and behavior/activity between hydrocephalic and control mice. The open field behavior test is one of the oldest, most extensively used, and simplest measures of mouse and rat behavior. It reflects "emotional" status (e.g. stress) and exploration [177, 181]. The open field apparatus records activity in three dimensions and allows complete automation of activity scoring. Factors such as environmental conditions, surgery and drug treatments may have effects on the performance of open field testing, however no single component measured in the open field test is reflective of one only factor [177]. Factors such as illness can lead to increased aggression, hypoactivity or hypersensitivity to handling [177]. An initial stage of exploration might be expected to be followed by a decrease in activity in a normal healthy animal as a consequence of habituation to the environment [177]. In a hydrocephalic animal the overall level of activity could be lower than in controls if they had severe neurologic impairment. Alternately, if there are memory deficits then the activity level might increase because environmental habituation did not occur. The results of open field testing in the present experiment were inconclusive; we were unable to recognize any pattern of behavioral differences between the adult control and hydrocephalic mice at either time point despite resting postural abnormalities in the juvenile hydrocephalic mice.

Locomotion is a complex behavior affected by the functional status of many different brain systems including the cerebellum, the telencephalic dopaminergic system, the corticospinal pathways, and the peripheral axon / muscle unit (i.e. muscle weakness) [180]. Beam walking measures the motor coordination and balance of mice as they traverse a narrow beam to reach an enclosed safety platform [180]. The rotorod/accelerod is a widely used test of balance and coordination task performed on a rotating rod [180]. We did not notice any differences between our control and hydrocephalic mice. In this laboratory the behavioral tests have been optimized for juvenile rats (up to 45g body weight). Perhaps a smaller diameter rod or a faster speed would have discriminated between the groups

In our laboratory we are mainly concerned with the progression of chronic hydrocephalus, therefore our primary objective is obtain a longer survival time frame than 5 days. Since mice injected with 25% kaolin showed such a rapid decline in health after 5 days, we followed up our next batch of animals with a decrease to 10 μL of 20% kaolin. These mice appeared to be in better health on day 5 and most survived until day 14, which is the end of our study timeframe. We built on these findings and injected the following group of mice with 10μL of 10% kaolin. These animals developed hydrocephalus after 2 days, and their general health and appearance was better than the previous two groups. The animals were well groomed and showed no signs of neurological impairment. This data suggests that a suspension of 10% kaolin at a volume of 10μL, is sufficient for inducing hydrocephalus in adult mice and a volume of 5μL for juveniles. One plausible explanation for this is that a less viscous suspension allows for better spread of the kaolin in the subarachnoid space and less brainstem compression.

Conclusions

My second goal was to induce hydrocephalus in young and adult CD1 mice using the percutaneous (closed) cisterna magna kaolin injection method. This would allow use of transgenic or knockout mice for further study of other aspects of hydrocephalus. We hypothesized that our results would be similar to those seen in the rat model. In the present experiment we progressively altered the kaolin concentration and volume based on the hypothesis that a less viscous solution would allow better spread of the kaolin and therefore would result in a lesser degree of brainstem compression. It is the opinion of this author that a suspension of 10% kaolin at a volume of 5-10μL is sufficient for inducing hydrocephalus in mice. Based on these observations, we can conclude that in this common outbred strain of CD1 mice, hydrocephalus can be successfully induced in both adult and juveniles. However I do have some reservations regarding the efficacy of this method. The challenge lies in the accuracy of the injection. It is the experience of this author, that when an injection is not completely within the cisterna magna, the injection results in a failure. In these mice, we can see evidence of the misplaced injections on MR imaging and when we dissect the animal. In addition to the challenge of injection location accuracy, there are difficulties in estimating the appropriate injection depth. Since mice have a very small 4^{th} ventricle and a tight posterior fossa, the potential to inject to deep (i.e. into the brainstem) is elevated. I suspect that this is the cause for the high acute mortality rate in adult mice.

Although rats and mice share similar anatomy, there seems to be less difficulty in

utilizing this method for young rats. A juvenile rat has the body weight equal to an adult mouse, approximately 40-50 grams. However the size of the cisterna magna is larger in the rat and thus the injection procedure is more forgiving. In this author's experience, injections that are slightly off centre still produce ventriculomegaly in young rats, although not as severe as those injected properly. Therefore it is reasonable to conclude that although this method has proven to successfully induce hydrocephalus in both juvenile and adult mice, the investigator must exercise caution when deciding to work with mice. We suggest that this method is easier to use on larger species, such as rats.

Chapter 4: Fluorescent dextran tracers and MR imaging demonstrate inconsistent blood-brain barrier disruption in young rats with kaolin-induced hydrocephalus

Introduction

In hydrocephalus, dilation of the cerebral ventricles leads to CSF diffusion across the ependyma causing periventricular edema. Disruption of the blood-brain barrier (BBB) as a consequence of hydrocephalus has been suggested, but there are inconsistencies demanding more experimentation [33]. As documented in the Chapter 1, previous studies of blood brain barrier permeability *in vivo* and *in situ* have utilized radiological and fluorescent tracer molecules to identify regions of disruption [182]. Fluorescein-isothiocyanate (FITC)-dextrans are very useful tracers for studying vascular permeability in nervous tissue, as capillaries of the cerebral cortex are impermeable to FITC-D tracers as small as 3kDa [12, 97, 98]. Gadolinium diethylenetriamine penta-acetate (Gd-DTPA) is a low molecular weight (590 Da) magnetic resonance (MR) imaging contrast agent well suited for delineating blood-brain barrier disruption and is used regularly clinically for this purpose [84, 183]. Ultrastructural evidence of BBB alteration (increased transendothelial vesicles) has been reported [184, 185], but these studies lack appropriate controls. Infusion of large tracers (including 125I-albumin (66kDa) [186], horseradish peroxidase (40kDa) [91] and microperoxidase (1900Da) [92], into the cerebral ventricles of animals with kaolin-induced hydrocephalus failed to demonstrate disruptions of the BBB, although ionic lanthanum (139Da) appears to retrospectively cross endothelial tight junctions to a greater degree in hydrocephalus [94]. Recently Turgut (2007) reported BBB disruption in kaolin induced hydrocephalic rats, using histology, biochemical analysis and a gamma camera, and suggested that this breakdown is due to the oxidative stress induced by the induction of kaolin [187]. Based on the conflicting literature we decided to pursue the topic of hydrocephalus and BBB disruption further. We

hypothesized that hydrocephalus induced by injection of kaolin into the cisterna magna of young rats would lead to blood brain barrier disruption as detected by efflux of lysine-fixable fluorescent dextran tracers into brain parenchyma and contrast enhanced MR imaging [183].

Materials and Methods

Animal Preparation

All animals were treated in accordance with the guidelines of the Canadian Council on Animal Care and protocols were approved by the University of Manitoba Animal Ethics Committee. Thirty male Sprague-Dawley rats 3 weeks of age were used. Animals were placed randomly into 2 groups of 15, each consisting of 10 rats injected with sterile kaolin and 5 controls, which received no kaolin. Animals were anesthetized with isoflurane (1.5% in oxygen). The head and neck were shaved and cleaned with Hibitane. With the neck flexed to maximize exposure to the foramen magnum, under aseptic conditions, a 0.30 ml syringe with 30-gauge needle was used for injection of 0.035 ml sterile kaolin suspension (aluminum silicate; Sigma, St. Louis MO) (250 mg/ml in 0.9% saline). Animals were monitored during recovery from anesthetic, weighed daily, and observed for signs of neurological impairment. Rats were housed 2 or 3 to a cage and allowed food and water freely.

MR Imaging and Gd-DTPA Administration

At 7 days (group 1) or 21 days (group 2) post-kaolin injection, MR analysis was performed on all rats from group 1 to establish onset of hydrocephalus. Magnetic resonance (MR) studies were performed using a Bruker Biospec/3 MR scanner equipped with a 21-cm bore magnet operating at a field of 7 Tesla (Karlsruhe, Germany) to obtain T1-weighted images of the brain in the coronal plane. Rats were imaged with a volume coil 32mm in diameter. The slice thickness was 1mm with an interslice gap of 1mm. The in-plane voxel resolution was 0.117mm x 0.117mm. The recovery time was 600ms, echo time 13ms, and the number of slices was 6.

Just prior to MR imaging the rats were anesthetized with 1.5–2% isoflurane in oxygen. Gd-DTPA was injected as a bolus (0.4mmol/kg, volume range 0.1-0.2mL) through a 30 gauge tail vein cannula while the rat was anesthetized and undisturbed in the magnet. The use of a stable tail-vein catheter allowed the intravenous administration of the Gd-DTPA while avoiding repositioning of the animal in the magnet. A set of pre-contrast T1-weighted images was obtained before the injection, and another set of contrast enhanced T1-weighted images was obtained 10 and 20 minutes post-Gd-DTPA injection. The ventricle size was calculated by ventricle area divided by total brain area on slices #5 and #6 (which include the frontal horns of the lateral ventricles). The percent intensity increase due to contrast enhancement was calculated voxel by voxel using the T1-weighted MR images obtained pre- and 20-minute post-Gd-DTPA injection as ((20min post-contrast image – pre-contrast image) / pre-contrast image) x 100% [183]. T1-weighted images were used to draw regions of interest (ROIs) omitting the ventricles. ROIs outlining the entire cerebrum and ventricular system were taken from pre-contrast

enhanced T1-weighted images (TE = 134ms) (Marevisi software; National Research Council, Canada). These ROIs were then superimposed onto the calculated percent enhancement images to quantify the average percent intensity increase within the entire brain parenchyma (see Figure 11). These methods have been previously described in detail [183].

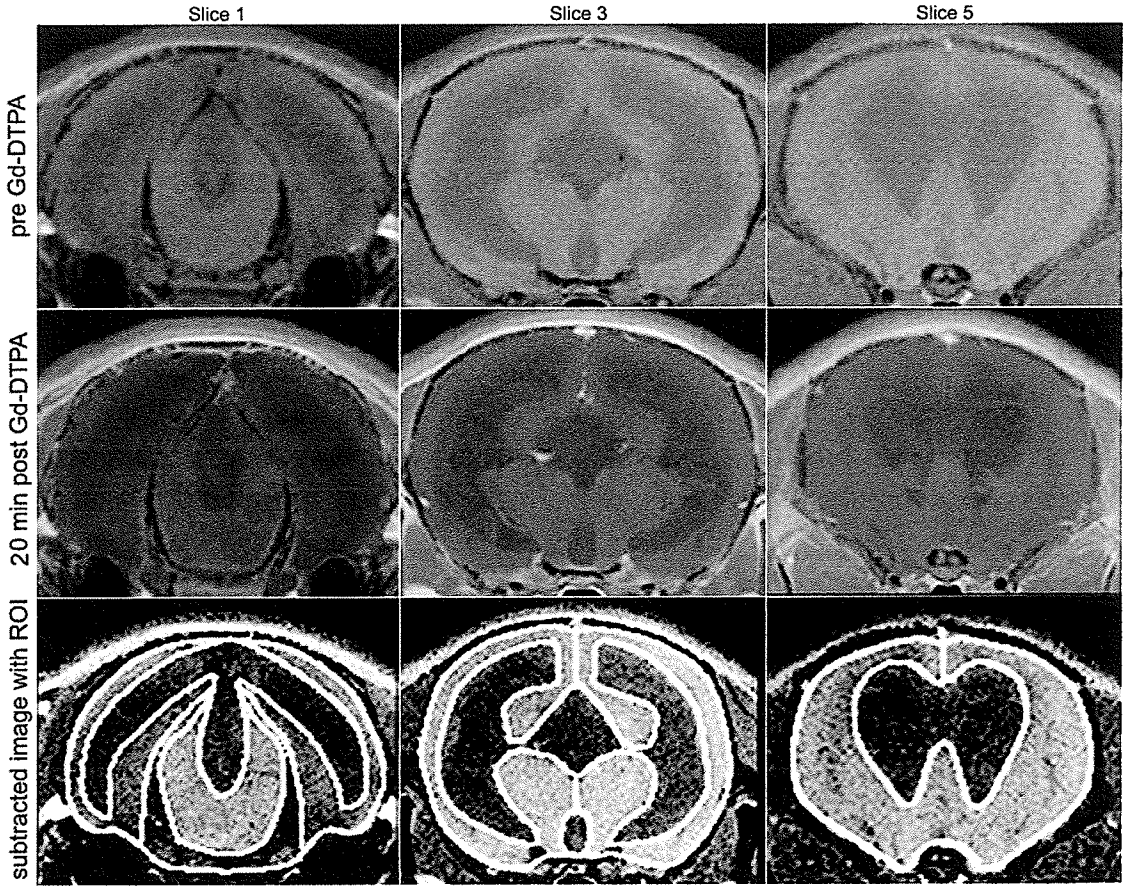

Figure 11: Coronal magnetic resonance (MR) images slices (T1 weighted) prior to (top row) and 20 minutes after (middle row) intravenous administration of Gd-DTPA to a hydrocephalic rat. Increased signal contrast is calculated by subtracting the first image set from the second set and then regions of interest (ROI) are superimposed onto calculated percent difference images (bottom row) to allow numeric calculation of the mean change for brain parenchyma. For all brains, six slices were obtained, but only three are shown for illustrative purposes.

Tracer Injection and Tissue Processing

Following MR imaging, a combination of dextran tracers (Texas Red 10,000mw and Fluorescein 500,000mw; Invitrogen Molecular Probes, CA, USA) at a dosage of 5 mg/100g body weight in sterile saline at a volume of 300-500μL, was injected into the cardiac left ventricle of anesthetized animals and allowed to circulate for 60 seconds, based on previous studies [188-190]. Rats were then perfusion-fixed with 3% paraformaldehyde, brains were removed and fixed in 3% paraformaldehyde. Brains were divided into three coronal slices by cutting at the levels of the optic chiasm and the mamillary bodies. Brain sections were embedded in paraffin and cut in 6μM sections for microscopic analysis. Sections were dewaxed, dehydrated in a graded ethanol series, dipped briefly in xylene, mounted with Permount and cover-slipped. Sections from each level were stained with hematoxylin and eosin for assessment of morphologic details.

Immunohistochemistry

To address an additional minor hypothesis that caveolin expression might be upregulated in regions of BBB breakdown [191] slides from each brain were immunostained using the following protocol. Sections were pretreated with 0.5% pepsin in 0.01 M HCl for 30 minutes at 37°C then rinsed, endogenous peroxidases were quenched with 3% hydrogen peroxide in methanol solution for 30 minutes. Sections were blocked with 10% sheep serum in PBS with 0.02% sodium dodecyl sulfate (SDS) for 30 minutes at room temperature in a humid chamber. Monoclonal anti-caveolin-1 (diluted 1:15; clone #2297; Becton-Dickenson Biosciences, Mississauga, ON, Canada) was

applied overnight at 4°C. Secondary antibody 1:500 biotinylated sheep anti-mouse in 1% BSA-PBST was applied for 2 hours at room temperature followed by streptavidin/HRP for 30 minutes, then diaminobenzidine. Negative control included omission of primary antibody.

Microscopic analysis

Tissues were examined under fluorescence epi-illumination at 40x, 100x, 200x and 400x magnification, blinded to the duration of hydrocephalus (it is not possible to blind control vs. hydrocephalics). The regions of tracer leakage were determined without reference to the MR results. In the present study, BBB opening and vascular leakage of the FITC-dextran was defined when there was clear evidence of fluorescence outside of the vessel lumen. Regions of tracer leakage were plotted onto a diagram of the brain and then were compared to the MR imaging results.

Statistical analysis

Data from each group of animals are reported as the mean ± standard error of the mean (SEM). Ventricle size index was calculated on the anterior MR slice #5 immediately anterior to the third ventricle. Ventricle/brain ratio was calculated by total ventricle area (mm^2) / total brain area (mm^2).

Results

Induction of hydrocephalus

All animals tolerated the procedures well with 100% induction of hydrocephalus among injected animals and no deaths. Ventricular dilation was variable in hydrocephalic animals, with a calculated brain to ventricle ratio of 0.21±0.02 (mean ± SEM) with a range of 0.11 to 0.28 in animals at 7 days post injection, and 0.32±0.07 with a range of 0.13 to 0.60 in animals at 21 days post injection. Control animals had ventricle to brain ratios of 0.001 in both groups (Figure 12).

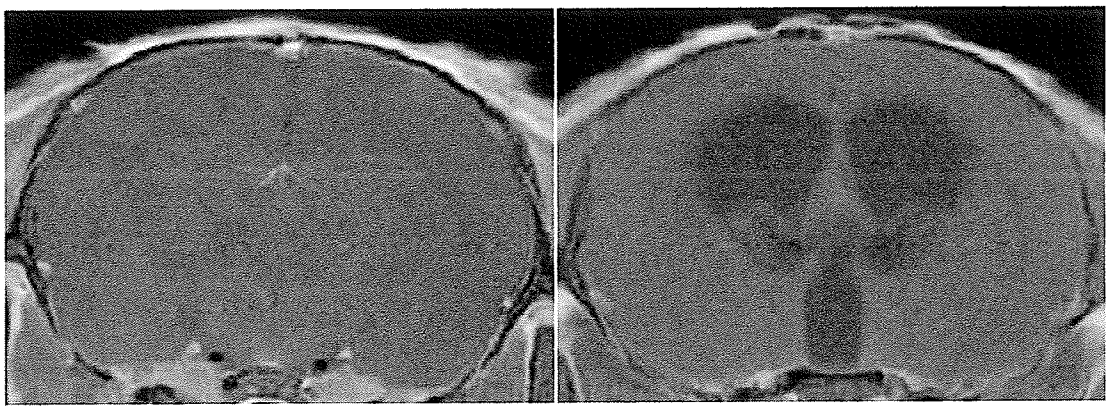

Figure 12: T1-weighted MR images showing coronal slices through rat brains at the level of the frontal horns of the lateral ventricles. In a 3-week-old control rat the ventricles are barely visible (left panel; ventricle size index 0.001). Kaolin injected at 3 weeks of age is associated with marked enlargement of the lateral and third ventricles by 7 days (right panel; ventricle size index 0.22).

MR imaging

MR imaging was conducted prior to the Gd-DTPA injection, and again 10 and 20 minutes post-Gd-DTPA injection. Unprocessed images were visually evaluated and no areas of signal enhancement were obvious. On the calculated difference images from the 20 minute post-Gd-DTPA scan we observed signal enhancement of the lining surrounding the frontal horns of the lateral ventricles in 7 hydrocephalics and 2 controls as shown in Figure 13.

The average pixel intensity in the entire brain was determined to be 13% greater after Gd-DTPA in control and hydrocephalic animals, excluding the area within the ventricles. This likely reflects circulating intravascular Gd-DTPA. Using threshold calculations we displayed pixels whose intensity increased >20% above control value (Figure 14 a, b). Control animals did not display any regions of pixel intensity above this value. Among the 20 hydrocephalic rats, 10 displayed focal changes after image calculations were performed (7 days post-injection n=7; 21 days post-injection n=3). These changes were only located on slices #1 or #2 (5.7 and 4.8 mm posterior to bregma respectively) in the periventricular region of the lateral ventricular horns, and posterior hypothalamic regions surrounding the third ventricle, as well as some regions of the posterior limbic or auditory cortex. There were only 1 or 2 focal leakage spots evident per animal on either slice #1 or #2 but not on both. The sizes of the leakages were 1-1.5 mm in diameter. There was no obvious difference between rats 7 and 21 days post kaolin injection despite increasing destruction of the white matter. This suggests that BBB disruption is not progressive or dependent on ventricle size.

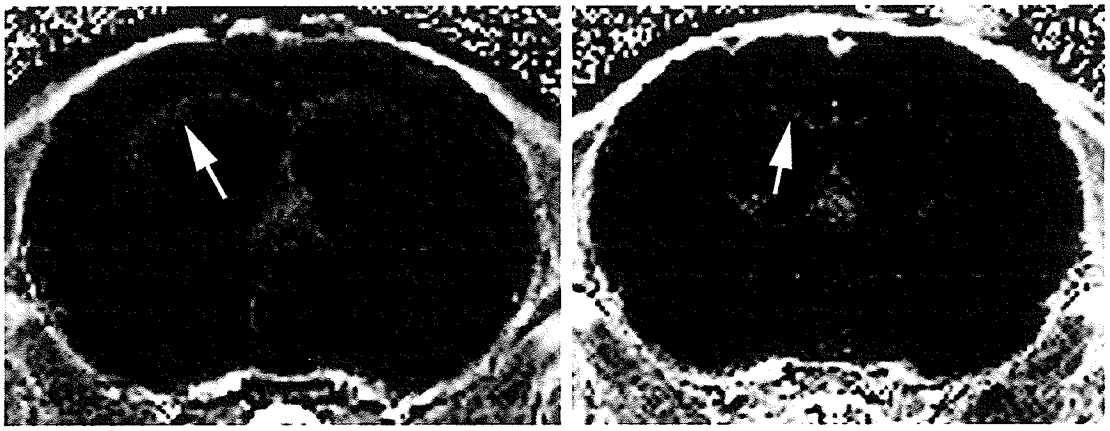

Figure 13: T1-weighted MR images showing coronal slices through two hydrocephalic rat brains (7 days post-kaolin injection) at the level of the frontal horns, 20 minutes after intravenous injection of Gd-DTPA. In these two examples, a rim of increased signal intensity surrounds the frontal horns of the lateral ventricle (arrows).

Microscopy

In all brains including controls, blood vessel lumens and choroid plexus exhibited strong red and green fluorescence following FITC-D perfusion. The ependymal lining of the ventricles also exhibited brighter fluorescence than the surrounding parenchyma, which is consistent with Gd-enhancement seen on MR. All hydrocephalic animals displayed regions of 10,000mw tracer leakage, while there was no evidence of either tracer leakage in any of the control animals. The regions of brain parenchyma that displayed tracer extravasation include the frontal and posterior periventricular white matter and the thalamus surrounding the third ventricle. There was no evidence of tracer leakage in the cortex, striatum or hippocampus. Nineteen hydrocephalic animals displayed 1 focus of extravasation per slide examined and one hydrocephalic animal showed 3 foci in one section. Generally vessels larger than capillaries with thin walls, probably veins, could be identified near the extravasation sites. Only one hydrocephalic animal (with moderate ventricular dilatation) displayed evidence of the larger (500,000mw) tracer at a single site. This might be attributed to a broken vessel at the time of sacrifice. There was no evidence of hemorrhage at these sites. The size of the extravasation foci was no more than 50μm and they were only visible at 200x magnification or greater. These regions corresponded relatively well with the calculated regions of Gd-DTPA leakage from the MR analysis, which displayed regions of enhancement in the periventricular zone on slices #1 or 2 (Figure14 c, d).

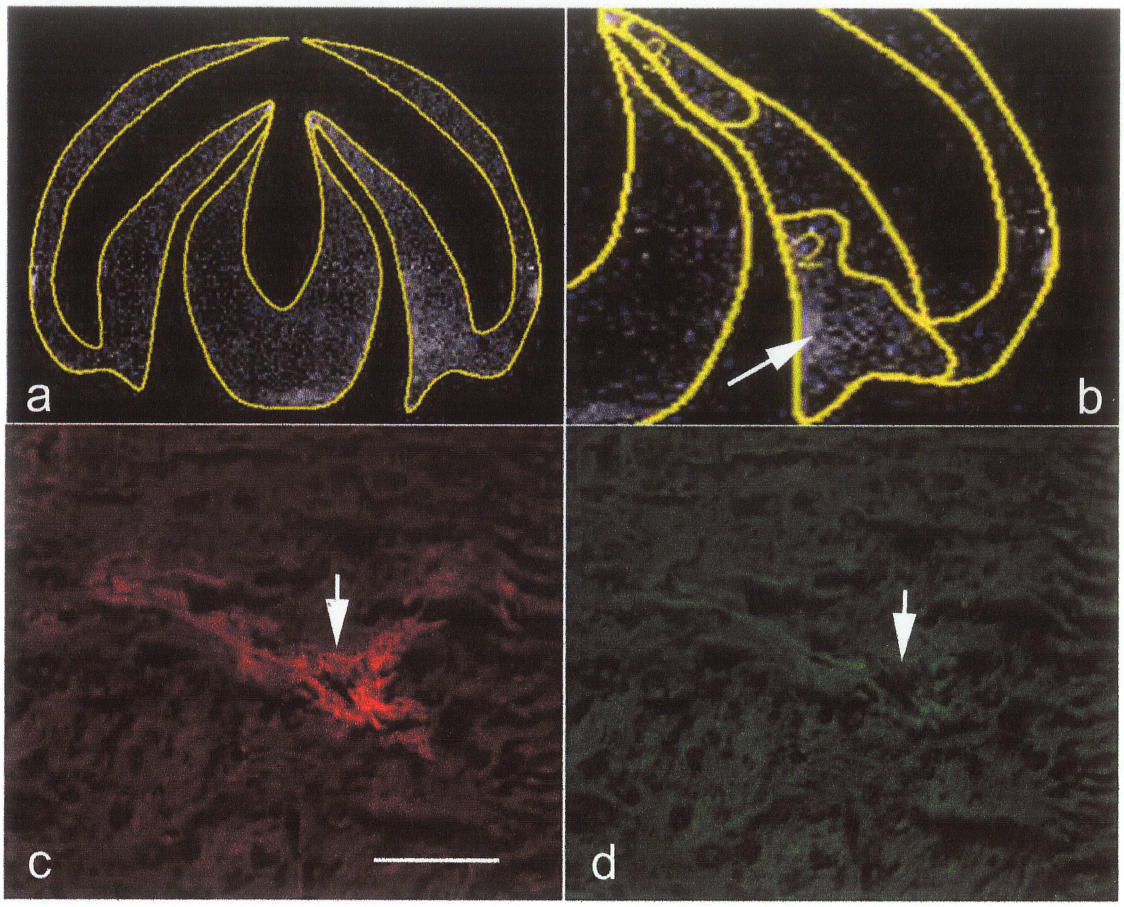

Figure 14: Subtracted MR image from a hydrocephalic rat 7 days post-kaolin injection with threshold adjusted to show only pixels whose intensity increased >20% (a- slice 1). Aggregates of bright pixels are indicative of regions where Gd-DTPA has leaked from the vasculature, e.g. close up of inferior temporal region (arrow in b). Fluorescence photomicrograph of corresponding location to signal enhanced region shows extravasated 10kDa Texas Red – dextran tracer into surrounding tissue (c), but no obvious extravasation of 500kDa Fluorescein - dextran tracer (d). Bar = 100 μm for c and d.

Caveolin-1 expression

Caveolin-1 immunoreactivity was observed in the endothelial cells lining all surface and choroid plexus vessels of hydrocephalic and control rats as shown in figure 15; this is consistent with previous reports [191]. There was also immunostaining in the endothelium of scattered parenchymal vessels, most prominent in the larger penetrating arteries and veins at the base of the brain, and approximately half of the capillaries. Vessels of hydrocephalic brains showed variable increases in immunostaining in scattered vessels of the cortex, striatum and white matter, however these regions did not specifically correspond with the regions where blood-brain barrier damage was noted with the resonance imaging or fluorescent analysis methods.

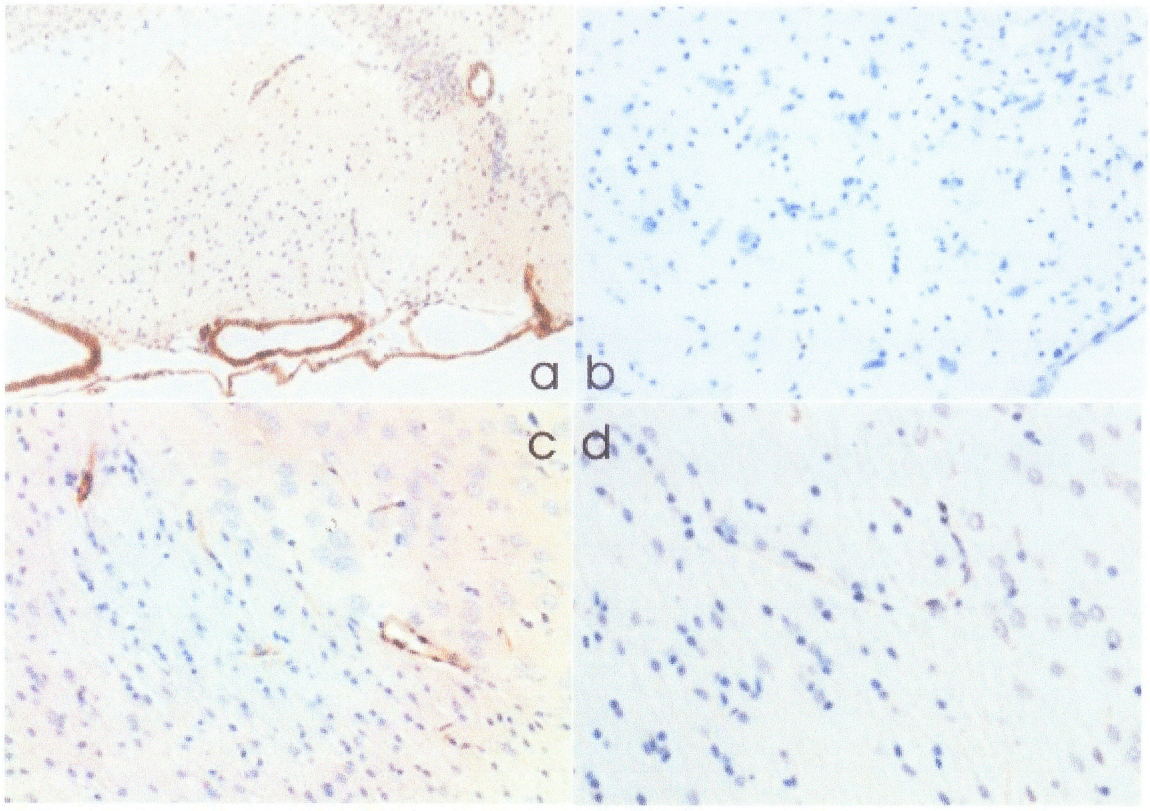

Figure 15: Immunostaining of rat brain for caveolin-1. Control (a) shows positive immunostaining (dark brown reaction product) of larger and penetrating vessels at base of brain (20x magnification). Negative control in (b) shows no labeling of vessels. Hydrocephalic rat brain at 6 weeks post-kaolin displays variable increases in immunostaining in scattered vessels of white matter (c, 40x; d, 60x magnification). The regions of positive staining did not correspond with regions of noted blood-brain barrier disruption.

Discussion

Hydrocephalus causes the ventricles within the brain to dilate while stretching and distorting the periventricular axons. It is possible that this mechanical stress damages scattered capillaries and veins. Our observations regarding the permeability of blood vessels in normal rat brain are consistent with previous studies [192, 193]. Our data suggest that blood brain-barrier integrity can be focally disrupted when young rats become hydrocephalic. However, there was no evidence that the change was progressive or dependent on the severity of hydrocephalus suggesting that the damage is random rather than systemic. It is possible that this mechanical stress randomly disrupts scattered veins. That is supported by the frequent observation of small collections of periventricular hemosiderin in this model. Since we did not see evidence of widespread Gd-DTPA leakage, we can rule out diffuse capillary dysfunction. The thalamic sites of leakage are more surprising because there is very little local distortion in the hydrocephalic rats. Perhaps that reflects venous backpressure due to restriction at the major outflow routes, for example on the surface of the distorted brain.

Tracer extravasation into brain parenchyma can occur through two principal mechanisms: through the endothelial cell (transcellular) or between the cells (paracellular) [92, 94]. The transcellular pathway permits entry by passive diffusion, but only neutral lipophilic substances with a molecular weight of less than 450 Da can gain access by this mechanism [194]. Under normal conditions, the paracellular space is almost completely obstructed by tight junctions that prevent passage of substances with a molecular weight of >180 Da [194]. It has been suggested that these pathways are altered

in hydrocephalus. Protein tracers such as HRP (40kDa) and microperoxidase (1900Da) that have been perfused into the ventricles, move along the extracellular space and pass through vesicles in the endothelial cytoplasm but not through tight junctions [86, 94, 195]. Electron microscopic studies on microvasculature describe separations of the endothelial cell tight junctions in hydrocephalic animal models [92, 94]. Dextrans have no affinity for specific carrier-mediated transport systems and are not transported in pinocytotic vesicles across the endothelium, nor are they lipophilic. There are several advantages to using dextrans as permeability tracers. They are 1) particulate, therefore quantitative analysis is possible, 2) they are stainable for electron microscopy, and 3) they are available in a wide variety of molecular sizes [97, 98, 188]. For these reasons, fluorochrome-conjugated dextrans are useful in determining "pore" size in neural vessels and in pathological situations where there is the possibility of a graded increase in vascular permeability [98].

Additional options for *in vivo* tracer experiments include ionic lanthanum (139 Da) and sodium fluorescein (342 Da). Lanthanum is the smallest marker visible by electron microscopy, however it is often lost from tissue during fixation and washing. Some studies suggest that lanthanum penetrates a few tight junctions, but it does not pass through to the basement membrane [196, 197]. Others have found lanthanum in the extracellular space and in the interendothelial clefts of hydrocephalic rats [94]. There is also evidence that lanthanum particles penetrate through tight junctions and pass into the intercellular space from the lumen during cardiac perfusion [94]. Additional tracer studies report effective use of sodium fluorescein (342 Da) for BBB examination, as it also does

not cross the intact blood-brain barrier [99, 102]. However, sodium fluorescein is a substrate for at least 2 groups of transporters at the BBB: multidrug resistance proteins (MRPs) and organic ion transporters (OATs) [198]. Therefore the extravasation of sodium fluorescein into brain parenchyma can be affected by both the integrity of the tight junctions as well as the expression/activity of these transporters [101, 199].

The observations regarding the permeability of blood vessels in normal brain are consistent with previous studies which suggest that tracers as small as 3kDa, do not typically cross the normal intact blood brain barrier [192, 193]. Our data suggests that blood brain-barrier maintenance and integrity can be influenced and disrupted when animals become hydrocephalic. However, there was no evidence that the change was progressive or dependent on the severity of hydrocephalus, suggesting that the damage is random rather than systemic.

MR contrast agent gadolinium (Gd-DTPA; 590 Da) has been documented to visualize regions of BBB disruption [101, 183, 200-202]. Gd-DTPA is biologically inert and passively diffuses into tissues throughout the extracellular space, with a half-life in blood and urine of approximately 20 minutes [203]. The short half-life of Gd-DTPA and the predominately renal elimination suggest that the compound has very little if any interaction within the body and does not dissociate *in vivo* [203]. The very high hydrophilicity, the charge, and the large molecular weight of Gd-DTPA (590 Da), all account for its exclusion by biologic barriers such as cell membranes. Gd-DTPA remains within the extracellular space and does not to penetrate the normal blood-brain barrier. From the pharmacokinetic and *in vitro* proton relaxation data for Gd-DTPA, is has been

documented that an *in vivo* dose of 0.1 -0.5 mmol/kg produces significant tissue enhancement on NMR images [203]. There is also a documented absence of cardiotoxicity [204]. In the present study we demonstrated with MR imaging, multiple foci of Gd-DTPA entry into hydrocephalic brains as well as along the ventricle lining. The latter might reflect leak through the choroid plexus where there is no BBB. Repeated MR imaging in the same animal at separate time points might have shown that the sites of leakage were transient.

We investigated the possibility of using quantitative analysis methods to determine the amount of tracer present in our samples, however concluded that these methods are not beneficial for this study for the following reasons. Methods such as capillary depletion, which offer a quantitative measure of the amount of tracer in the brain parenchyma versus what is in the vasculature, may not be sensitive enough to detect such minor leakage in such a relatively large volume of brain parenchyma. The capillary depletion method can be used to quantify transcytosis of proteins and other substances (tracers) through the blood brain barrier. It is done by infusing a perfusate solution into the brain vasculature of a living animal. The perfusate solution includes a radio-labeled test compound and a radio-labeled marker compound. The perfused brain is removed from the animal and then homogenized. The homogenize brain is then separated into a microvasculature fraction containing red blood cells, brain nuclei and vasculature; and a supernatant fraction which is completely devoid of vasculature. The net volume of the distribution of the test compound in the supernatant is calculated and corrected to provide an accurate measure of tracer transcytosis through the blood brain barrier that is not

simply bound to or associated with brain capillaries. These results are compared with samples of perfusion fluid (blood or plasma) for determination of perfusate tracer concentrations [205, 206]. This method is not suitable for this study because as animals progressively become more hydrocephalic, the volume of brain tissue decreases. This would decrease our total brain volume to be homogenized and would result in having to pool samples together in order to obtain a workable volume of homogenate.

Other methods, such as the use of radio-iodinated serum albumin (RISA) to obtain a quantitative estimate of BBB permeability, have advantages and disadvantages. An injection of 10μCi RISA is given intravenously and blood must be collected at regular intervals, via the femoral artery and vein, before, during and after the administration of RISA. An intravenous injection of Evans blue is administered 10 minutes prior to termination of the experiment. A thoracotomy is performed and the animal is perfused with saline to remove RISA from the vessels. The brain is removed and divided into regions of interest and are put into pre-weighed scintillation vials, which are re-weighed to determine the weight of brain and blood. Radioactivity of the samples is determined using a gamma counter and the sum of the radioactivity is used to calculate the leakage of RISA in the brain. The amount of RISA leakage is expressed as a percentage of plasma radioactivity yielding an accurate estimate of the percent of protein transfer [95]. The disadvantage of this method is that the tracer cannot be detected by visual examination and therefore has to be used in combination with a visible tracer such as Evans blue in order to identify regions of BBB disruption before selecting the areas to measure

radioactivity. This method also provides no information about how BBB breakdown occurs at the tissue level [95].

There are a variety of other techniques available for estimating the uptake of substances into the brain, each with their own advantages and disadvantages. *In vivo* methods of intravenous injection and brain sampling remain the reference for brain uptake studies because it is highly sensitive and fully represents the actual physiological conditions [207]. Brain uptake index (BUI) is a quick procedure and utilizes a wide range of injectate compositions, however it is relatively insensitive compared to intravenous injections, as it is difficult to measure minute volumes. The BUI is a single pass method which employs a rapid bolus injection of a radio-labeled test substance and reference substance, which does not cross the intact BBB, into the carotid artery of an anesthetized animal [207]. After 2 seconds passage time through brain capillaries, brain uptake can be measured by tissue sampling after decapitation. This short time interval excludes systemic recirculation and also minimizes potential washout. A simple calculation of BUI represents a relative measure substance uptake in the brain. BUI measurements are particularly suitable for substances with moderate to high BBB permeability. The shortfalls of the BUI method have been addressed by the development of brain perfusion methods [207].

Brain perfusion methods are more sensitive than BUI and allows for estimation of flow rates, however it is technically more difficult to administer. The perfusion of a physiological buffer containing the test compound is started after the ligation of the

carotid artery. In addition to the manipulation of the perfusate composition, control of the flow rate is possible. The longer exposure of the brain capillary bed to the perfusate, compared to the single pass technique, increases the sensitivity. Perfusion times can be increased to as high as 1 hour by the addition of oxygen carriers to buffer [207, 208]. The relatively slow transport process versus the rapid carrier mediated transport, makes brain perfusion a good method when characterizing receptor-mediated uptake. However this method is prone to artifacts and it is difficult to distinguish between the fraction of a test compound that is associated with the endothelial cells, versus that which has passed through the endothelium and entered the brain parenchyma. This analysis is possible with the capillary depletion method.

Quantitative autoradiography (QAR) is an imaging process that determines the *in situ* localization of radio-labeled compounds in tissues of laboratory animals [209]. Animals are euthanized, quick frozen, embedded in a frozen carboxy-methylcellulose matrix, and cryosectioned. Autoradiography refers to the original technique of exposing the whole-body sections to X-ray film, which produces a photographic image [210]. Phosphor imaging produces digital images of radioactivity distributed within the tissues. Autoradiography produces photographic quality images of high resolution and clarity; however, it is more difficult to obtain quantitative results from these images and the sample-to-film exposure time is relatively long (weeks) [209]. The new technology of direct nuclear counting and imaging is also an accurate way to directly acquire quantitative autoradiographic images from whole-body sections [211]. QAR uses radioactive tracers, typically ^{14}C, administered intravenously, which allow for evaluations

of regional permeability surface area (PS) and serve as the reference for external detection techniques, such as MRI. Although time consuming, QAR provides excellent spatial resolution but does not provide any proof of the integrity of the tracer. However it is difficult to measure BBB PS products less than 10μL using this method. To date, QAR with radio-labeled tracers and Gd-DTPA enhanced MRI remain the best approaches for localizing and quantifying BBB disruption, although histologic approaches might still be more sensitive [200, 201].

We demonstrated with MR imaging multiple foci of Gd-DTPA entry into hydrocephalic brains as well as along the ventricle lining. The latter might reflect leak through the choroid plexus where there is no BBB. Repeated MR imaging in the same animal at separate time points might have shown that the sites of leakage were transient. With respect to the fluorescent-dextran conjugates, other authors use a looser definition of BBB opening with the appearance of a widespread haze of fluorescence evidence of tracer leakage[193, 200, 201]. Although these may indeed be regions of leakage, we considered only distinct fluorescence around a vessel to represent BBB breakdown, assuming that broad diffusion would not have occurred in the brief time after injection. We acknowledge that we might exclude areas where there is minor leakage, however we expect that the MR method would be sensitive to that.

The nature of caveolin-1 immunostaining has been reported previously [191, 212]. The chronic exposure of endothelial cells to shear stress (as in arterial hypertension) is known to increase plasma membrane levels of caveolin-1 due to the redistribution of

caveolin-1 from the Golgi complex to the plasma membrane, accompanied by an increase in surface density of caveolae [213-215]. Nag (2007) reported an increase in caveolin-1 expression in rats with cold-injury beginning at 12 hours post-injury with moderate increases at 2 and 4 days post-injury [191]. We had hypothesized that an increase might also be seen in hydrocephalic rats in association with the BBB changes or the white matter edema, but no obvious changes were observed.

Conclusion

My final goal was to study blood-brain barrier (BBB) disruption in hydrocephalic rats. We hypothesized that hydrocephalic rats would have some degree BBB disruption evident on Gadolinium-contrast enhanced T1-weighted MR imaging, and that we could correlate the regions of MR enhancement with histological evidence of BBB disruption using fluorescent-conjugate-dextran tracers. In the present study we demonstrated with two methods that hydrocephalic rats had focal areas of randomly distributed foci of BBB disruption to tracers >10,000 but <500,000 Da. There was no generalized change even in the periventricular white matter where axonal damage is known to be progressive. This suggests that hydrocephalus is not associated with a generalized disturbance in the BBB. The mechanism of this disruption could be random rupture of small veins as their tensile strength is exceeded. Alternately, but less likely (based upon the morphology of vessels at sites of leakage), proliferating capillaries might be transiently permeable as they grow. This observation is important be because it supports the idea that periventricular water

content changes are due to alterations of CSF-extracellular fluid fluxes. Furthermore, if pharmacologic agents are to be used to protect the white matter, they must be able to traverse the normal BBB.

Chapter 5: General Summary and Future Directions

Chapter 5: General Summary and Future Directions

My first objective was to improve upon the kaolin model of hydrocephalus in rats in order to reduce meningeal inflammation. The results of our biopolymer experiment indicate that the current model of cisterna magna injections of kaolin should still be considered to be the most reliable and efficient method for inducing obstructive hydrocephalus in rats. Although it causes a mild inflammatory reaction of the meninges, this is a caveat that one must be willing to accept; there appears to be no inflammation in the brain tissue itself. The kaolin model is reliable in producing ventriculomegaly and it is to some extent titratable. The kaolin injection method is also well tolerated by the animals and the development of hydrocephalus is constant and progressive, eventually reaching a compensated or plateau state relative to the age of injection. The survival rate is this model has been documented to be close to 100% and animals have been documented to survive up to 36 weeks post-injection [216]. There is the possibility that Matrigel offers a non-inflammatory alternative to kaolin. Future studies of this protein mixture, perhaps in a more concentrated form, should be conducted to address the possibility of reabsorption and the inconsistencies that we encountered.

My second objective was to determine whether the kaolin injection can be used to induce hydrocephalus that is survivable beyond the acute stage in young and adult CD1 mice. The changes in these mice are similar to those documented in rats, such as development of an enlarged head, decreased body weight, and ventricular dilatation. However there are technical issues that need to be considered. Decreasing the

concentration of the kaolin suspension from 25% to 10% produced a better survival rate in both young and adult mice, resulting in less compression of the brainstem and a better spread of the kaolin within the subarachnoid space. This is probably important because the fourth ventricle and subarachnoid compartment in mice is extremely small, leaving little room for viscous kaolin suspension to spread. Future studies on a further decrease in kaolin concentration may provide better survival rates, although it remains to be documented whether the degree of ventricular dilatation would become compromised. Refinement of this model will allow use of transgenic mice for addressing hypotheses with respect to the role of individual gene function in hydrocephalus.

My third objective was to test the hypothesis that induction of hydrocephalus would lead to some degree of blood-brain barrier disruption, and that this disruption would be detectable using contrast MR imaging and fluorescent microscopy. Using the reliable model of kaolin hydrocephalus in young rats, we demonstrated with two methods, the presence of focal areas of randomly distributed BBB disruption to tracers >10,000 but <500,000 Da. There was no generalized change even in the periventricular white matter where axonal damage is known to be progressive, which suggests that hydrocephalus is not associated with a generalized disturbance in the BBB. This observation is important because it supports the idea that periventricular water content changes are due to alterations of CSF-extracellular fluid fluxes. The mechanism could result in the random rupture of small veins as their tensile strength is exceeded. The issue of BBB permeability evaluation and investigation are essential when developing drugs for treatment of central nervous system disorders. It is very important to understand to

what extent these molecules enter the CNS because if pharmacologic agents are to be used to protect the white matter, they must first be able to traverse the normal BBB.

Chapter 6: References

1. Del Bigio, M.R., *Pathophysiologic consequences of hydrocephalus.* Neurosurg Clin N Am, 2001. **12**(4): p. 639-649.
2. Eklund, A., et al., *Assessment of cerebrospinal fluid outflow resistance.* Med Biol Eng Comput, 2007. **45**(8): p. 719-35.
3. Moody, D.M., *The blood-brain barrier and blood-cerebral spinal fluid barrier.* Semin Cardiothorac Vasc Anesth, 2006. **10**(2): p. 128-31.
4. Czosnyka, M., et al., *Cerebrospinal fluid dynamics.* Physiol Meas, 2004. **25**(5): p. R51-76.
5. Greitz, D., T. Greitz, and T. Hindmarsh, *A new view on the CSF circulation with the potential for pharmacological treatment of childhood hydrocephalus.* Acta Paediatr., 1997. **86**: p. 125-132.
6. Greitz, D., *The bulk flow model cannot explain communicating hydrocephalus and must be replaced by a new concept.* Childs Nerv Syst, 2007.
7. Chiafery, M., *Care and management of the child with shunted hydrocephalus.* Pediatr Nurs, 2006. **32**(3): p. 222-5.
8. Moyes, P.D., *Hydrocephalus.* Can Med Assoc J, 1968. **98**(7): p. 354-8.
9. Koh, L., G. Nagra, and M. Johnston, *Properties of the lymphatic cerebrospinal fluid transport system in the rat: impact of elevated intracranial pressure.* J Vasc Res, 2007. **44**(5): p. 423-32.
10. Johnston, M. and C. Papaiconomou, *Cerebrospinal fluid transport: a lymphatic perspective.* News Physiol Sci, 2002. **17**: p. 227-230.
11. Boulton, M., et al., *Contribution of extracranial lymphatics and arachnoid villi to the clearance of a CSF tracer in the rat.* Am J Physiol, 1999. **276**(3 Pt 2): p. R818-R823.
12. Zhang, J., M.A. Williams, and D. Rigamonti, *Genetics of human hydrocephalus.* J Neurol, 2006.
13. Stein, S.C. and L. Schut, *Hydrocephalus in myelomeningocele.* Childs Brain, 1979. **5**(4): p. 413-419.
14. Holt, P.J. and W.C. Allan, *The natural history of ventricular dilatation in neonatal intraventricular hemorrhage and its therapeutic implications.* Ann. Neurol., 1981. **10**: p. 293-294.
15. Hochwald, G.M., *Animal models of hydrocephalus: recent developments.* Proc. Soc. Exp. Biol. Med., 1985. **178**: p. 1-11.
16. Rizvi, R. and Q. Anjum, *Hydrocephalus in children.* J Pak Med Assoc, 2005. **55**(11): p. 502-7.
17. Paine, R.S., *Hydrocephalus.* Pediatr Clin North Am, 1967. **14**(4): p. 779-96.
18. Strecker, E.P. and A.E. James, Jr., *The evaluation of cerebrospinal fluid flow and absorption: clinical and experimental studies.* Neuroradiology, 1973. **6**(4): p. 200-205.
19. Strecker, E.P., M. Bush, and A.E. James, Jr., *Cerebrospinal fluid imaging as a method to evaluate communicating hydrocephalus in dogs.* Am J Vet Res, 1973. **34**(1): p. 101-104.

20. Pattisapu, J.V., *Etiology and clinical course of hydrocephalus.* Neurosurg Clin N Am, 2001. **12**(4): p. 651-9, vii.
21. McLone, D.G., *Cerebrospinal fluid pathways in a murine mutant.* Childs Brain, 1979. **5**(3): p. 293-303.
22. McLone, D.G., *Hydrocephalus.* Pediatr Neurosurg, 2000. **33**(2): p. 57.
23. McLone, D.G., *Congenital malformations of the central nervous system.* Clin Neurosurg, 2000. **47**: p. 346-77.
24. Aravabhumi, S. and K.L. Izzo, *Sensory and motor deficits of central nervous system origin.* Clin Podiatr Med Surg, 1989. **6**(4): p. 707-43.
25. Del Bigio, M.R., *Neuropathological changes caused by hydrocephalus.* Acta Neuropathol (Berl), 1993. **85**(6): p. 573-585.
26. Rubin, R.C., et al., *Reconstitution of the cerebral cortical mantle in shunt-corrected hydrocephalus.* Dev Med Child Neurol Suppl, 1975(35): p. 151-156.
27. Rubin, R.C., et al., *Hydrocephalus: II. Cell number and size, and myelin content of the pre-shunted cerebral cortical mantle.* Surg Neurol, 1976. **5**(2): p. 115-118.
28. Penfield, W. and A.R. Elvidge, *Hydrocephalus and the atrophy of cerebral compression.*, in *Cytology and Cellular Pathology of the Nervous System*, W. Penfield, Editor. 1932, P.S. Hoebner: New York. p. 1201-1217.
29. Russell, D.S., *Observations on the pathology of hydrocephalus.* Med. Res. Council Special Report Ser., 1949. **265**: p. 1-138.
30. Del Bigio, M.R., *The ependyma: a protective barrier between brain and cerebrospinal fluid.* Glia, 1995. **14**: p. 1-13.
31. Bryan, J.H.D., R.L. Hughes, and T.J. Bates, *Brain development in the hydrocephalic-polydactyl, a recessive pleiotropic mutant in the mouse.* Virchows Arch. A, 1977. **374**: p. 205-214.
32. Shimizu, A. and M. Koto, *Ultrastructure and movement of the ependymal and tracheal cilia in congenitally hydrocephalic WIC-Hyd rats.* Childs Nerv Syst, 1992. **8**(1): p. 25-32.
33. McAllister, J.P., II and P. Chovan, *Neonatal hydrocephalus. Mechanisms and consequences.* Neurosurg Clin N Am, 1998. **9**(1): p. 73-93.
34. Banizs, B., et al., *Dysfunctional cilia lead to altered ependyma and choroid plexus function, and result in the formation of hydrocephalus.* Development, 2005. **132**(23): p. 5329-39.
35. Bush, A., *Primary ciliary dyskinesia.* Acta Otorhinolaryngol Belg, 2000. **54**(3): p. 317-24.
36. De, S.N., *A study of the changes in the brain in experimental internal hydrocephalus.* J. Pathol. Bacteriol., 1950. **62**: p. 197-208.
37. Hochwald, G.M., et al., *Cerebrospinal fluid production and histological observations in animals with experimental obstructive hydrocephalus.* Exp. Neurol., 1969. **25**: p. 190-199.
38. Ogata, J., et al., *Light and electron microscopic studies of experimental hydrocephalus. Ependymal and subependymal areas.* Acta Neuropathol (Berl), 1972. **21**(3): p. 213-223.
39. Weller, R.O., et al., *The effects of hydrocephalus upon the developing brain. Histological and quantitative studies of the ependyma and subependyma in hydrocephalic rats.* J Neurol Sci, 1978. **36**(3): p. 383-402.

40. Torvik, A. and A.E. Stenwig, *The pathology of experimental obstructive hydrocephalus. Electron microscopic observations.* Acta Neuropathol., 1977. **38**: p. 21-26.
41. Torvik, A., R. Bhatia, and V.S. Murthy, *Transitory block of the arachnoid granulations following subarachnoid haemorrhage. A postmortem study.* Acta Neurochir. Wien., 1978. **41**: p. 137-146.
42. Weller, R.O., *Pathology of cerebrospinal fluid and interstitial fluid of the CNS: significance for Alzheimer disease, prion disorders and multiple sclerosis.* J Neuropathol Exp Neurol, 1998. **57**(10): p. 885-894.
43. Dominguez-Pinos, M.D., et al., *Ependymal denudation and alterations of the subventricular zone occur in human fetuses with a moderate communicating hydrocephalus.* J Neuropathol Exp Neurol, 2005. **64**(7): p. 595-604.
44. Miller, J.M. and J.P. McAllister, 2nd, *Reduction of astrogliosis and microgliosis by cerebrospinal fluid shunting in experimental hydrocephalus.* Cerebrospinal Fluid Res, 2007. **4**(1): p. 5.
45. McAllister, J.P., 2nd, et al., *Effects of congenital hydrocephalus on the hypothalamic gonadotrophin-releasing hormone system.* Neurosurg Focus, 2007. **22**(4): p. E4.
46. McAllister, J.P., 2nd, *Neuronal damage in hydrocephalus.* J Neurosurg, 2006. **104**(5 Suppl): p. 297-8; discussion 298.
47. Del Bigio, M.R. and J.E. Bruni, *Periventricular pathology in hydrocephalic rabbits before and after shunting.* Acta Neuropathol (Berl), 1988. **77**(2): p. 186-195.
48. Mataro, M., et al., *Functional and magnetic resonance imaging correlates of corpus callosum in normal pressure hydrocephalus before and after shunting.* J Neurol Neurosurg Psychiatry, 2006.
49. Feinberg, D.A., *Functional magnetic resonance imaging. Application to degenerative brain disease and hydrocephalus.* Neuroimaging Clin N Am, 1995. **5**(1): p. 125-34.
50. da Silva, M.C., et al., *Reduced local cerebral blood flow in periventricular white matter in experimental neonatal hydrocephalus-restoration with CSF shunting.* J Cereb Blood Flow Metab, 1995. **15**(6): p. 1057-1065.
51. Hill, A. and J.J. Volpe, *Decrease in pulsatile flow in the anterior cerebral arteries in infantile hydrocephalus.* Pediatrics, 1982. **69**: p. 4-7.
52. Goh, D. and R.A. Minns, *Intracranial pressure and cerebral arterial flow velocity indices in childhood hydrocephalus: current review.* Childs Nerv Syst, 1995. **11**(7): p. 392-396.
53. Dombrowski, S.M., et al., *Chronic hydrocephalus-induced changes in cerebral blood flow: mediation through cardiac effects.* J Cereb Blood Flow Metab, 2006. **26**(10): p. 1298-310.
54. Braun, K.P.J., et al., *NMR spectroscopic evaluation of cerebral metabolism in hydrocephalus: A review.* Neurol. Res., 2000. **22**(1): p. 51-64.
55. Massicotte, E.M. and M.R. Del Bigio, *Human arachnoid villi response to subarachnoid hemorrhage: possible relationship to chronic hydrocephalus.* J. Neurosurg., 1999. **91**(1): p. 80-84.

56. Socci, D.J., et al., *Evidence that oxidative stress is associated with the pathophysiology of inherited hydrocephalus in the H-Tx rat model.* Exp Neurol, 1999. **155**(1): p. 109-117.
57. Brinker, T., et al., *Sinusoidal intrathecal infusion for assessment of CSF dynamics in kaolin-induced hydrocephalus.* Acta Neurochir., 1998. **140**(10): p. 1069-1075.
58. Sato, O., et al., *Microcirculatory changes in experimental hydrocephalus: morphological and physiological studies.*, in *Hydrocephalus*, K. Shapiro, A. Marmarou, and H. Portnoy, Editors. 1984, Raven Press: New York. p. 215-230.
59. Del Bigio, M.R. and J.E. Bruni, *Changes in periventricular vasculature of rabbit brain following induction of hydrocephalus and after shunting.* J Neurosurg, 1988. **69**(1): p. 115-120.
60. Glees, P., et al., *Fine structural features of the cerebral microvasculature in hydrocephalic human infants: correlated clinical observations.* Neurosurg Rev, 1989. **12**(4): p. 315-321.
61. Klinge, P.M., et al., *Cerebral hypoperfusion and delayed hippocampal response after induction of adult kaolin hydrocephalus.* Stroke, 2003. **34**(1): p. 193-199.
62. Higashi, K., et al., *Cerebral blood flow and metabolism in experimental hydrocephalus.* Neurol. Res., 1986. **8**: p. 169-176.
63. Jones, H.C., et al., *Progressive tissue injury in infantile hydrocephalus and prevention/reversal with shunt treatment.* Neurol. Res., 2000. **22**(1): p. 89-96.
64. Suda, K., et al., *Early ventriculoperitoneal shunt--effects on learning ability and synaptogenesis of the brain in congenitally hydrocephalic HTX rats.* Childs Nerv Syst, 1994. **10**(1): p. 19-23.
65. Brooks, D.J., et al., *Studies on cerebral oxygen metabolism, blood flow, and blood volume, in patients with hydrocephalus before and after surgical decompression, using positron emission tomography.* Brain, 1986. **109**(Pt 4): p. 613-628.
66. Shahar, E., et al., *Obstructive hydrocephalus-induced Parkinsonism. I: Decreased basal ganglia blood flow.* Pediatr. Neurol., 1988. **4**: p. 117-119.
67. Greitz, T.V.B., et al., *Pre- and postoperative evaluation of cerebral blood flow in low-pressure hydrocephalus.* J. Neurosurg., 1969. **41**: p. 644-651.
68. da Silva, M.C., et al., *High-energy phosphate metabolism in a neonatal model of hydrocephalus before and after shunting.* J Neurosurg, 1994. **81**(4): p. 544-553.
69. Shirane, R., et al., *Cerebral blood flow and oxygen metabolism in infants with hydrocephalus.* Child's Nerv. Syst., 1992. **8**: p. 118-123.
70. Kriebel, R.M., A.B. Shah, and J.P. McAllister, II, *The microstructure of cortical neuropil before and after decompression in experimental infantile hydrocephalus.* Exp Neurol, 1993. **119**(1): p. 89-98.
71. Hale, P.M., et al., *Improvement of cortical morphology in infantile hydrocephalic animals after ventriculoperitoneal shunt placement.* Neurosurgery, 1992. **31**(6): p. 1085-1096.
72. Kiefer, M., et al., *The ependyma in chronic hydrocephalus.* Childs Nerv Syst, 1998. **14**(6): p. 263-270.
73. Del Bigio, M.R., J.E. Bruni, and H.D. Fewer, *Human neonatal hydrocephalus. An electron microscopic study of the periventricular tissue.* J Neurosurg, 1985. **63**(1): p. 56-63.

74. Del Bigio, M.R. and J.E. Bruni, *Silicone oil-induced hydrocephalus in the rabbit.* Childs Nerv Syst, 1991. 7(2): p. 79-84.
75. Takei, F. and O. Sato, *Morphological analysis of progressive hydrocephalus and shunt-dependent arrested hydrocephalus.* Pediatr. Neurosurg., 1995. **23**: p. 246-253.
76. Del Bigio, M.R., *Biological reactions to cerebrospinal fluid shunt devices: a review of the cellular pathology.* Neurosurgery, 1998. **42**(2): p. 319-325.
77. Nakada, J., et al., *Changes in the cerebrovascular bed in experimental hydrocephalus: an angio-architectural and histological study.* Acta Neurochir., 1992. **114**: p. 43-50.
78. Harris, N.G., H.C. Jones, and S. Patel, *Ventricle shunting in young H-Tx rats with inherited congenital hydrocephalus: a quantitative histological study of cortical grey matter.* Childs Nerv Syst, 1994. **10**(5): p. 293-301.
79. Abbott, N.J. and I.A. Romero, *Transporting therapeutics across the blood-brain barrier.* Mol Med Today, 1996. **2**(3): p. 106-13.
80. Goldstein, G.W. and A.L. Betz, *The blood-brain barrier.* Sci Am, 1986. **255**(3): p. 74-83.
81. Fry, M., T.D. Hoyda, and A.V. Ferguson, *Making sense of it: roles of the sensory circumventricular organs in feeding and regulation of energy homeostasis.* Exp Biol Med (Maywood), 2007. **232**(1): p. 14-26.
82. Mayhan, W.G., *Regulation of blood-brain barrier permeability.* Microcirculation, 2001. **8**(2): p. 89-104.
83. Abbott, N.J., L. Ronnback, and E. Hansson, *Astrocyte-endothelial interactions at the blood-brain barrier.* Nat Rev Neurosci, 2006. 7(1): p. 41-53.
84. Rebeles, F., et al., *Blood-brain barrier imaging and therapeutic potentials.* Top Magn Reson Imaging, 2006. **17**(2): p. 107-16.
85. Sada, Y., et al., *Immunohistochemical study on blood-brain barrier in congenitally hydrocephalic HTX rat brain.* Zentralbl Pathol, 1994. **140**(4-5): p. 289-298.
86. Weller, R.O. and J. Mitchell, *Cerebrospinal fluid edema and its sequelae in hydrocephalus.* Adv Neurol, 1980. **28**: p. 111-123.
87. Perry, J.H., *Alterations in blood-brain barrier in experimental hydrocephalus.*, in *Disorders of the Developing Nervous System*, W.S. Fields and M.M. Desmond, Editors. 1961, Charles C. Thomas: Sprinfield, IL. p. 326-342.
88. Marlin, A.E., et al., *On the movement of fluid through the brain of hydrocephalic cats.* Neurology, 1976. **26**(12): p. 1159-1163.
89. Hochwald, G.M., et al., *Sodium exchange between blood, brain, and CSF in normal and hydrocephalic cats.* J Neurosci Res, 1977. **3**(4): p. 267-273.
90. Lux, W.E., Jr., et al., *Periventricular water content. Effect of pressure in experimental chronic hydrocephalus.* Arch. Neurol., 1970. **23**: p. 475-479.
91. Ogata, J., et al., *Distribution of intraventricular horseradish peroxidase in normal and hydrocephalic cat brains.* J. Neuropathol. Exp. Neurol., 1972. **31**: p. 454-463.
92. Nakagawa, Y., J. Cervos-Navarro, and J. Artigas, *A possible paracellular route for resolution of hydrocephalic edema.* Acta Neuropathol., 1984. **64**: p. 122-128.

93. Kuwahara, S., et al., *Spatial and temporal expression of P-glycoprotein in the congenitally hydrocephalic HTX rat brain.* Pathol Res Pract, 1996. **192**(5): p. 496-507.
94. Nakagawa, Y., J. Cervos-Navarro, and J. Artigas, *Tracer study on a paracellular route in experimental hydrocephalus.* Acta Neuropathol., 1985. **65**(3-4): p. 247-254.
95. Nag, S., *Blood-brain barrier permeability using tracers and immunohistochemistry.* Methods Mol Med, 2003. **89**: p. 133-144.
96. Nakamura, S., Y. Oi, and N. Moriyasu, *[Electron microscopic study of choroid plexus in experimentally induced hydrocephalic dog (author's transl)].* No Shinkei Geka, 1975. **3**(2): p. 153-62.
97. Thorball, N., *FITC-dextran tracers in microcirculatory and permeability studies using combined fluorescence stereo microscopy, fluorescence light microscopy and electron microscopy.* Histochemistry, 1981. **71**(2): p. 209-33.
98. Hulstrom, D. and E. Svensjo, *Intravital and electron microscopic study of bradykinin-induced vascular permeability changes using FITC-dextran as a tracer.* J Pathol, 1979. **129**(3): p. 125-33.
99. D'Amato, R., E. Wesolowski, and L.E. Smith, *Microscopic visualization of the retina by angiography with high-molecular-weight fluorescein-labeled dextrans in the mouse.* Microvasc Res, 1993. **46**(2): p. 135-42.
100. Zhang, Y.W. and M.R. Del Bigio, *Growth-associated protein-43 is increased in cerebrum of immature rats following induction of hydrocephalus.* Neuroscience, 1998. **86**(3): p. 847-854.
101. Hawkins, B.T. and R.D. Egleton, *Fluorescence imaging of blood-brain barrier disruption.* J Neurosci Methods, 2006. **151**(2): p. 262-267.
102. Tervo, T. and A. Palkama, *Innervation of the rabbit cornea. A histochemical and electron-microscopic study.* Acta Anat (Basel), 1978. **102**(2): p. 164-75.
103. Khan, O.H. and M.R. Del Bigio, *Experimental models of hydrocephalus (Chapter 26)*, in *Handbook of Experimental Neurology: Methods and Techniques in Animal Research (ISBN-10: 0521838142)*, T. Tatlisumak and M. Fisher, Editors. 2006, Cambridge University Press: Cambridge. p. 457-471.
104. Nakayama, D.K., et al., *Correction of congenital hydrocephalus in utero I. The model: intracisternal kaolin produces hydrocephalus in fetal lambs and rhesus monkeys.* J Pediatr Surg, 1983. **18**(4): p. 331-338.
105. Edwards, M.S., et al., *Kaolin-induced congenital hydrocephalus in utero in fetal lambs and rhesus monkeys.* J Neurosurg, 1984. **60**(1): p. 115-122.
106. Schurr, P.H., R.L. McLaurin, and F.D. Ingraham, *Experimental studies on the circulation of the cerebrospinal fluid and methods of producing communicating hydrocephalus in the dog.* J. Neurosurg., 1953. **10**: p. 515-525.
107. Sahar, A., G.M. Hochwald, and J. Ransohoff, *Alternate pathway for cerebrospinal fluid absorption in animals with experimental obstructive hydrocephalus.* Exp. Neurol., 1969. **25**(2): p. 200-206.
108. Jouet, M. and S. Kenwrick, *Gene analysis of L1 neural cell adhesion molecule in prenatal diagnosis of hydrocephalus.* Lancet, 1995. **345**(8943): p. 161-162.

109. Rosenthal, A., M. Jouet, and S. Kenwrick, *Aberrant splicing of neural cell adhesion molecule L1 mRNA in a family with X-linked hydrocephalus.* Nature Genetics, 1992. **2**: p. 107-112.
110. Bruni, J.E., et al., *Hereditary hydrocephalus in laboratory animals and humans.* Exp. Pathol., 1988. **35**: p. 239-249.
111. Davy, B.E. and M.L. Robinson, *Congenital hydrocephalus in hy3 mice is caused by a frameshift mutation in Hydin, a large novel gene.* Hum Mol Genet, 2003. **12**(10): p. 1163-1170.
112. Raimondi, A.J., et al., *The pathophysiology and morphology of murine hydrocephalus in hy-3 and Ch mutants.* Surg. Neurol., 1973. **1**: p. 50-55.
113. Bronson, R.T. and P.W. Lane, *Hydrocephalus with hop gait (hyh): a new mutation on chromosome 7 in the mouse.* Brain Res Dev Brain Res, 1990. **54**(1): p. 131-136.
114. Paez, P., et al., *Patterned Neuropathologic Events Occurring in hyh Congenital Hydrocephalic Mutant Mice.* J Neuropathol Exp Neurol, 2007. **66**(12): p. 1082-1092.
115. Davson, H., K. Welch, and M.B. Segal, *The Physiology and Pathophysiology of the Cerebrospinal Fluid.* 1987, Edinburgh: Churchill Livingstone. 1013.
116. Rolf, B., M. Kutsche, and U. Bartsch, *Severe hydrocephalus in L1-deficient mice.* Brain Res., 2001. **891**(1-2): p. 247-252.
117. Galbreath, E., et al., *Overexpression of TGF-beta 1 in the central nervous system of transgenic mice results in hydrocephalus.* J Neuropathol Exp Neurol, 1995. **54**(3): p. 339-349.
118. Cohen, A.R., et al., *Characterization of a model of hydrocephalus in transgenic mice.* J. Neurosurg., 1999. **91**(6): p. 978-988.
119. Tada, T., M. Kanaji, and S. Kobayashi, *Induction of communicating hydrocephalus in mice by intrathecal injection of human recombinant transforming growth factor-beta 1.* J. Neuroimmunol., 1994. **50**(2): p. 153-158.
120. Ibanez-Tallon, I., et al., *Dysfunction of axonemal dynein heavy chain Mdnah5 inhibits ependymal flow and reveals a novel mechanism for hydrocephalus formation.* Hum Mol Genet, 2004. **13**(18): p. 2133-2141.
121. Torikata, C., C. Kijimoto, and M. Koto, *Ultrastructure of respiratory cilia of WIC-Hyd male rats. An animal model for human immotile cilia syndrome.* Am J Pathol, 1991. **138**(2): p. 341-347.
122. Chen, J., et al., *Mutation of the mouse hepatocyte nuclear factor/forkhead homologue 4 gene results in an absence of cilia and random left-right asymmetry.* J Clin Invest, 1998. **102**(6): p. 1077-1082.
123. Daniel, G.B., et al., *Communicating hydrocephalus in dogs with congenital ciliary dysfunction.* Dev. Neurosci., 1995. **17**(4): p. 230-235.
124. al-Shroof, M., et al., *Ciliary dyskinesia associated with hydrocephalus and mental retardation in a Jordanian family.* Mayo Clin Proc, 2001. **76**(12): p. 1219-1224.
125. Picco, P., et al., *Primary hypothyroidism and 131I-MIBG therapy in neuroblastoma.* Lancet, 1993. **342**(8862): p. 57.
126. Greenstone, M.A., et al., *Hydrocephalus and primary ciliary dyskinesia.* Arch Dis Child, 1984. **59**(5): p. 481-2.

127. Miyazawa, T., et al., *A rat model of spontaneously arrested hydrocephalus. A behavioural study.* Childs Nerv Syst, 1997. **13**(4): p. 189-193.
128. Oi, S., et al., *Experimental models of congenital hydrocephalus and comparable clinical problems in the fetal and neonatal periods.* Childs Nerv Syst, 1996. **12**(6): p. 292-302.
129. Dandy, W.E., *Experimental hydrocephalus.* Ann. Surg., 1919. **70**(2): p. 129-142.
130. Cherian, S., et al., *The pathogenesis of neonatal post-hemorrhagic hydrocephalus.* Brain Pathol, 2004. **14**(3): p. 305-311.
131. Johanson, C.E., et al., *Altered formation and bulk absorption of cerebrospinal fluid in FGF-2-induced hydrocephalus.* Am. J. Physiol., 1999. **277**(1): p. R263-R271.
132. Nakazato, F., et al., *Disturbed spatial learning of rats after intraventricular administration of transforming growth factor-beta 1.* Neurol Med Chir (Tokyo), 2002. **42**(4): p. 151-156.
133. Ohmiya, M., et al., *Administration of FGF-2 to embryonic mouse brain induces hydrocephalic brain morphology and aberrant differentiation of neurons in the postnatal cerebral cortex.* J. Neurosci. Res., 2001. **65**(3): p. 228-235.
134. Dixon, W.E. and H. Heller, *Experimentelle Hypertonie durch Eröhung des intrakaniellen Druckes.* Arch. Exp. Pathol. Pharmakol., 1932. **166**: p. 265-275.
135. Shinoda, M. and L. Olson, *Immunological aspects of kaolin-induced hydrocephalus.* Int J Neurosci, 1997. **92**(1-2): p. 9-28.
136. Del Bigio, M.R. and Y.W. Zhang, *Cell death, axonal damage, and cell birth in the immature rat brain following induction of hydrocephalus.* Exp Neurol, 1998. **154**(1): p. 157-169.
137. Khan, O.H., T.L. Enno, and M.R. Del Bigio, *Brain damage in neonatal rats following kaolin induction of hydrocephalus.* Exp Neurol, 2006. **200**(2): p. 311-320.
138. Bloch, O., et al., *Accelerated progression of kaolin-induced hydrocephalus in aquaporin-4-deficient mice.* J Cereb Blood Flow Metab, 2006.
139. Hatta, J., et al., *Heavy water inhibiting the expression of transforming growth factor-beta1 and the development of kaolin-induced hydrocephalus in mice.* J Neurosurg, 2006. **104**(4 Suppl): p. 251-258.
140. Williams, M.A., et al., *Priorities for hydrocephalus research: report from an NIH-sponsored workshop.* J. Neurosurg., 2007. **107 (5 Suppl. Pediatrics)**: p. 345-357.
141. Del Bigio, M.R., *Cellular damage and prevention in childhood hydrocephalus.* Brain Pathol, 2004. **14**(3): p. 317-324.
142. Cherian, S.S., et al., *Posthemorrhagic ventricular dilation in the neonate: development and characterization of a rat model.* J Neuropathol Exp Neurol, 2003. **62**(3): p. 292-303.
143. Emonard, H., et al., *Reconstituted basement-membrane matrix modulates fibroblast activities in vitro.* J Cell Physiol, 1987. **133**(1): p. 95-102.
144. Kleinman, H.K. and G.R. Martin, *Matrigel: basement membrane matrix with biological activity.* Semin Cancer Biol, 2005. **15**(5): p. 378-386.

145. Joosten, E.A., P.R. Bar, and W.H. Gispen, *Collagen implants and cortico-spinal axonal growth after mid-thoracic spinal cord lesion in the adult rat.* J Neurosci Res, 1995. **41**(4): p. 481-490.
146. Kassam, A., et al., *Use of Tisseel fibrin sealant in neurosurgical procedures: incidence of cerebrospinal fluid leaks and cost-benefit analysis in a retrospective study.* Neurosurgery, 2003. **52**(5): p. 1102-1105.
147. Buchta, C., et al., *Biochemical characterization of autologous fibrin sealants produced by CryoSeal and Vivostat in comparison to the homologous fibrin sealant product Tissucol/Tisseel.* Biomaterials, 2005. **26**(31): p. 6233-6241.
148. Weisman, R.A., et al., *Biochemical characterization of autologous fibrinogen adhesive.* Laryngoscope, 1987. **97**(10): p. 1186-1190.
149. Brothers, M.F., et al., *n-Butyl 2-cyanoacrylate--substitute for IBCA in interventional neuroradiology: histopathologic and polymerization time studies.* AJNR Am J Neuroradiol, 1989. **10**(4): p. 777-786.
150. Johnson, M.J., et al., *Development and characterization of an adult model of obstructive hydrocephalus.* J. Neurosci. Meth., 1999. **91**(1-2): p. 55-65.
151. Ayad, M., E. Eskioglu, and R.A. Mericle, *Onyx: a unique neuroembolic agent.* Expert Rev Med Devices, 2006. **3**(6): p. 705-715.
152. Del Bigio, M.R., C.R. Crook, and R. Buist, *Magnetic resonance imaging and behavioral analysis of immature rats with kaolin-induced hydrocephalus: pre- and postshunting observations.* Exp Neurol, 1997. **148**(1): p. 256-264.
153. Wisniewski, H., R.O. Weller, and R.D. Terry, *Experimental hydrocephalus produced by the subarachnoid infusion of silicone oil.* J Neurosurg, 1969. **31**(1): p. 10-14.
154. Go, K.G., et al., *Changes of ventricular ependyma and choroid plexus in experimental hydrocephalus, as observed by scanning electron microscopy.* Acta Neuropathol (Berl), 1976. **34**(1): p. 55-64.
155. Kassam, A., et al., *Use of Tisseel fibrin sealant in neurosurgical procedures: incidence of cerebrospinal fluid leaks and cost-benefit analysis in a retrospective study.* Neurosurgery, 2003. **52**(5): p. 1102-5; discussion 1105.
156. Menovsky, T., et al., *Stability of fibrin sealant in cerebrospinal fluid: an in vitro study.* Neurosurgery, 2002. **51**(6): p. 1453-1456.
157. Huang, N.F., et al., *Injectable biopolymers enhance angiogenesis after myocardial infarction.* Tissue Eng, 2005. **11**(11-12): p. 1860-1866.
158. Vakonakis, I. and I.D. Campbell, *Extracellular matrix: from atomic resolution to ultrastructure.* Curr Opin Cell Biol, 2007. **19**(5): p. 578-83.
159. Sajanti, J., et al., *Increase of collagen synthesis and deposition in the arachnoid and the dura following subarachnoid hemorrhage in the rat.* Biochim Biophys Acta, 1999. **1454**(3): p. 209-16.
160. Sajanti, J. and K. Majamaa, *Detection of meningeal fibrosis after subarachnoid haemorrhage by assaying procollagen propeptides in cerebrospinal fluid.* J Neurol Neurosurg Psychiatry, 1999. **67**(2): p. 185-8.
161. Abir, R., et al., *Morphological study of fully and partially isolated early human follicles.* Fertil Steril, 2001. **75**(1): p. 141-6.
162. Abir, R., et al., *Pilot study of isolated early human follicles cultured in collagen gels for 24 hours.* Hum Reprod, 1999. **14**(5): p. 1299-301.

163. de Vries, J., et al., *Histological effects of fibrin glue on nervous tissue: a safety study in rats.* Surg Neurol, 2002. **57**(6): p. 415-422.
164. Terasaka, S., et al., *Fibrin glue and polyglycolic Acid nonwoven fabric as a biocompatible dural substitute.* Neurosurgery, 2006. **58**(1 Suppl): p. ONS134-139.
165. Agarwal, A., A. Varma, and C. Sarkar, *Histopathological changes following the use of biological and synthetic glue for dural grafts: an experimental study.* Br J Neurosurg, 1998. **12**(3): p. 213-216.
166. Duffner, F., et al., *Combined therapy of cerebral arteriovenous malformations: histological differences between a non-adhesive liquid embolic agent and n butyl 2-cyanoacrylate (NBCA).* Clin Neuropathol, 2002. **21**(1): p. 13-17.
167. Germano, I.M., et al., *Histopathological follow-up study of 66 cerebral arteriovenous malformations after therapeutic embolization with polyvinyl alcohol.* J Neurosurg, 1992. **76**(4): p. 607-614.
168. Quisling, R.G., et al., *Histopathologic analysis of intraarterial polyvinyl alcohol microemboli in rat cerebral cortex.* AJNR Am J Neuroradiol, 1984. **5**(1): p. 101-104.
169. Murayama, Y., et al., *Nonadhesive liquid embolic agent for cerebral arteriovenous malformations: preliminary histopathological studies in swine rete mirabile.* Neurosurgery, 1998. **43**(5): p. 1164-1175.
170. Santos, N.C., et al., *Multidisciplinary utilization of dimethyl sulfoxide: pharmacological, cellular, and molecular aspects.* Biochem Pharmacol, 2003. **65**(7): p. 1035-1041.
171. Batiz, F., et al., *Clinical and neuropathological evolution of the hydrocephalus developed by the mutant mouse hyh.* Cerebrospinal Fluid Res, 2005. **2 Suppl 1**: p. S9.
172. Matsumoto, S., et al., *Comparative study of various models of experimental hydrocephalus.* Childs Brain, 1975. **1**(4): p. 236-242.
173. Khan, O.H., T. Enno, and M.R. Del Bigio, *Magnesium sulfate therapy is of mild benefit to young rats with kaolin-induced hydrocephalus.* Pediatr. Res., 2003. **53**(6): p. 970-976.
174. Khan, O.H., T. Enno, and M.R. Del Bigio, *Tacrolimus and cyclosporine are of no benefit to young rats with kaolin-induced hydrocephalus.* Pediatr Neurosurg, 2003. **39**(6): p. 309-313.
175. Moser, V.C., et al., *The IPCS Collaborative Study on Neurobehavioral Screening Methods: II. Protocol design and testing procedures.* NeuroToxicology, 1997. **18**(4): p. 929-938.
176. Del Bigio, M.R. and E.M. Massicotte, *Protective effect of nimodipine on behavior and white matter of rats with hydrocephalus.* J. Neurosurg., 2001. **94**(5): p. 788-794.
177. Crawley, J.N., et al., *Behavioral phenotypes of inbred mouse strains: implications and recommendations for molecular studies.* Psychopharmacology (Berl), 1997. **132**(2): p. 107-24.
178. Vestergaard, E., *Morphological Changes In The Lateral Ventricles Of The Mouse Brain During Growth.* Acta Anat (Basel), 1964. **59**: p. 315-26.

179. Sturrock, R.R., *A comparison of the processes of ventricular coarctation and choroid and ependymal fusion in the mouse brain.* J Anat, 1979. **129**(Pt 2): p. 235-42.
180. Karl, T., R. Pabst, and S. von Horsten, *Behavioral phenotyping of mice in pharmacological and toxicological research.* Exp Toxicol Pathol, 2003. **55**(1): p. 69-83.
181. DeFries, J.C., J.P. Hegmann, and M.W. Weir, *Open-field behavior in mice: evidence for a major gene effect mediated by the visual system.* Science, 1966. **154**(756): p. 1577-9.
182. Nag, S., *Blood-brain barrier permeability using tracers and immunohistochemistry.* Methods Mol Med, 2003. **89**: p. 133-44.
183. Schellenberg, A.E., et al., *Magnetic resonance imaging of blood-spinal cord barrier disruption in mice with experimental autoimmune encephalomyelitis.* Magn Reson Med, 2007. **58**(2): p. 298-305.
184. Castejon, O.J., *Electron microscopic study of capillary wall in human cerebral edema.* J. Neuropathol. Exp. Neurol., 1980. **49**: p. 296-328.
185. Hasan, M. and P. Glees, *Ultrastructural features of the human frontal cortex neurons of maturing and hydrocephalic cerebrum.* Arch. Ital. Anat. Embriol., 1990. **95**: p. 17-26.
186. Marlin, A.E., et al., *Kaolin-induced hydrocephalus impairs CSF secretion by the choroid plexus.* Neurology, 1978. **28**(9 Pt 1): p. 945-949.
187. Turgut, M., et al., *Melatonin ameliorates blood-brain barrier permeability, glutathione, and nitric oxide levels in the choroid plexus of the infantile rats with kaolin-induced hydrocephalus.* Brain Res, 2007. **1175**: p. 117-125.
188. Zhang, Y., et al., *Efflux transport of [3H]GABA across blood-brain barrier after cerebral ischemia-reperfusion in rats.* Zhongguo Yao Li Xue Bao, 1999. **20**(3): p. 223-6.
189. Gobel, U., et al., *Glucose utilization, blood flow and capillary density in the ventrolateral medulla of the rat.* Pflugers Arch, 1990. **416**(5): p. 477-80.
190. Gobel, U., H. Theilen, and W. Kuschinsky, *Congruence of total and perfused capillary network in rat brains.* Circ Res, 1990. **66**(2): p. 271-81.
191. Nag, S., R. Venugopalan, and D.J. Stewart, *Increased caveolin-1 expression precedes decreased expression of occludin and claudin-5 during blood-brain barrier breakdown.* Acta Neuropathol, 2007. **114**(5): p. 459-69.
192. Banerjee, S. and M.A. Bhat, *Neuron-glial interactions in blood-brain barrier formation.* Annu Rev Neurosci, 2007. **30**: p. 235-58.
193. Nagaraja, T.N., et al., *Acute leakage patterns of fluorescent plasma flow markers after transient focal cerebral ischemia suggest large openings in blood-brain barrier.* Microcirculation, 2008. **15**(1): p. 1-14.
194. Petty, M.A. and E.H. Lo, *Junctional complexes of the blood-brain barrier: permeability changes in neuroinflammation.* Prog Neurobiol, 2002. **68**(5): p. 311-23.
195. Brightman, M.W. and T.S. Reese, *Junctions between intimately apposed cell membranes in the vertebrate brain.* J. Cell Biol., 1969. **40**(3): p. 648-677.
196. Brightman, M.W., *Morphology of blood-brain interfaces.* Exp Eye Res, 1977. **25 Suppl**: p. 1-25.

197. Brightman, M.W. and T.S. Reese, *Junctions between intimately apposed cell membranes in the vertebrate brain.* J Cell Biol, 1969. **40**(3): p. 648-77.
198. Soodvilai, S., et al., *Acute regulation of OAT3-mediated estrone sulfate transport in isolated rabbit renal proximal tubules.* Am J Physiol Renal Physiol, 2004. **287**(5): p. F1021-9.
199. Hawkins, B.T. and T.P. Davis, *The blood-brain barrier/neurovascular unit in health and disease.* Pharmacol Rev, 2005. **57**(2): p. 173-185.
200. Knight, R.A., et al., *Quantitation and localization of blood-to-brain influx by magnetic resonance imaging and quantitative autoradiography in a model of transient focal ischemia.* Magn Reson Med, 2005. **54**(4): p. 813-21.
201. Knight, R.A., et al., *Acute blood-brain barrier opening in experimentally induced focal cerebral ischemia is preferentially identified by quantitative magnetization transfer imaging.* Magn Reson Med, 2005. **54**(4): p. 822-32.
202. Prior, M.J., et al., *MRI characterisation of a novel rat model of focal astrocyte loss.* Magma, 2004. **17**(3-6): p. 125-32.
203. Weinmann, H.-J., et al., *Characteristics of Gd-DTPA and new derivatives.*, in *Contrast Media in MRI: International Workshop.*, G. Bydder, et al., Editors. 1990, Medicom Europe: Bussum, Netherlands. p. 19-30.
204. Fobben, E.S., et al., *MR characteristics of subdural hematomas and hygromas at 1.5 T.* AJR Am J Roentgenol, 1989. **153**(3): p. 589-95.
205. Triguero, D., J. Buciak, and W.M. Pardridge, *Capillary depletion method for quantification of blood-brain barrier transport of circulating peptides and plasma proteins.* J Neurochem, 1990. **54**(6): p. 1882-8.
206. Rabin, O., et al., *Rapid brain uptake of manganese(II) across the blood-brain barrier.* J Neurochem, 1993. **61**(2): p. 509-17.
207. Bickel, U., *How to measure drug transport across the blood-brain barrier.* NeuroRx, 2005. **2**(1): p. 15-26.
208. Smith, Q.R., *A review of blood-brain barrier transport techniques.* Methods Mol Med, 2003. **89**: p. 193-208.
209. Solon, E.G. and L. Kraus, *Quantitative whole-body autoradiography in the pharmaceutical industry. Survey results on study design, methods, and regulatory compliance.* J Pharmacol Toxicol Methods, 2001. **46**(2): p. 73-81.
210. Ullberg, S., *Autoradiographical distribution and excretion studies with S35-labelled penicillin.* Proc Soc Exp Biol Med, 1954. **85**(4): p. 550-3.
211. Schweitzer, A., A. Fahr, and W. Niederberger, *A simple method for the quantitation of 14C-whole-body autoradiograms.* Int J Rad Appl Instrum [A], 1987. **38**(5): p. 329-33.
212. Virgintino, D., et al., *Expression of caveolin-1 in human brain microvessels.* Neuroscience, 2002. **115**(1): p. 145-52.
213. Boyd, N.L., et al., *Chronic shear induces caveolae formation and alters ERK and Akt responses in endothelial cells.* Am J Physiol Heart Circ Physiol, 2003. **285**(3): p. H1113-22.
214. Parton, R.G. and K. Simons, *The multiple faces of caveolae.* Nat Rev Mol Cell Biol, 2007. **8**(3): p. 185-94.

215. Rizzo, V., et al., *Recruitment of endothelial caveolae into mechanotransduction pathways by flow conditioning in vitro.* Am J Physiol Heart Circ Physiol, 2003. **285**(4): p. H1720-9.
216. Balasubramaniam, J. and M.R. Del Bigio, *Analysis of age-dependant alteration in the brain gene expression profile following induction of hydrocephalus in rats.* Exp Neurol, 2002. **173**(1): p. 105-113.